RADIO SCINTILLATION DUE TO DISCONTINUITIES IN THE INTERSTELLAR PLASMA DENSITY

H. C. LAMBERT[1]

Max-Planck-Institut für Radioastronomie
Auf dem Hügel 69, D-53121 Bonn, Germany

B. J. RICKETT[2]

Department of Electrical & Computer Engineering
University of California San Diego, La Jolla, CA 92093-0407

DRAFT: FEBRUARY 1, 2008

ABSTRACT

We develop the theory of interstellar scintillation as caused by an irregular plasma having a power-law spatial density spectrum with a spectral exponent of $\beta = 4$ corresponding to a medium with abrupt changes in its density. An "outer scale" is included in the model representing the typical scale over which the density of the medium remains uniform. Such a spectrum could be used to model plasma shock fronts in supernova remnants or other plasma discontinuities. We investigate and develop equations for the decorrelation bandwidth of diffractive scintillations and the refractive scintillation index and compare our results with pulsar measurements. We consider both a medium concentrated in a thin layer and an extended irregular medium. We conclude that the $\beta = 4$ model gives satisfactory agreement for many diffractive measurements, in particular the VLBI meaurements of the structure function exponent between 5/3 and 2. However, it gives less satisfactory agreement for the refractive scintillation index than does the Kolmogorov turbulence spectrum. The comparison suggests that the medium consists of a pervasive background distribution of turbulence embedded with randomly placed discrete plasma structures such as shocks or HII regions. This can be modeled by a composite spectrum following the Kolmogorov form at high wavenumbers and steepening at lower wavenumbers corresponding to the typical (inverse) size of the discrete structures. Such a model can also explain the extreme scattering events. However, lines of sight through the enhanced scattering prevalent at low galactic latitudes are accurately described by the Kolmogorov spectrum in an extended medium and do not appear to have a similar low-wavenumber steepening.

Subject headings: radiative transfer — ISM: general — pulsars: general

---

[1]e-mail: hlambert@mpifr-bonn.mpg.de

[2]e-mail: rickett@ece.ucsd.edu

1. INTRODUCTION

It is well known that radio waves propagating in the interstellar medium (ISM) are scattered by the irregularities in the Galactic electron density. The scattering in turn gives rise to a number of observable phenomena. Among others, these include angular broadening and intensity fluctuations (both in time and frequency) of compact radio sources. While a nuisance in many radio astronomical observations, these phenomena can be used to investigate the nature of the irregularities in the interstellar plasma density. These density irregularities are in turn believed to follow the fluctuations in the interstellar kinetic and magnetic energies. Ideally one would like to invert observations of radio scintillation and scattering to determine the statistics of the plasma density. As noted by Narayan (1992) this inverse problem is not well posed and one must rely on modeling methods. A complete prediction of scintillation observables requires an *a priori* knowledge of both the form of the spatial power spectrum of the electron density fluctuations and the distribution of the scattering material along the line of sight. For a given profile of the distribution of the scattering material, one may compare observations and predictions and so constrain the functional form of the spectrum. The power spectrum provides useful insight into the physics of the plasma irregularities. Hence a knowledge of the form of the density spectrum becomes central in both predicting scintillation phenomena and understanding the physics of the interstellar plasma. In this paper, we revisit the investigation of the form of the density spectrum.

A commonly used model for the density spectrum has been based on a power-law model with a large range between "inner" and "outer" scales (e.g. Rickett 1977):

$$P_{N_e}(q) = \frac{C_{N_e}^2(z)}{(q^2 + \kappa_o^2)^\beta} \exp\left[-\frac{q^2}{4\kappa_i^2}\right] . \qquad (1)$$

Here q is the magnitude of the three-dimensional wavenumber $\vec{q}$.

$C_{N_e}^2(z)$ denotes the strength of fluctuations (with a weak dependence on distance z). β is the spectral exponent, and $\kappa_i^{-1} = L_i$ and $\kappa_o^{-1} = L_o$ are the inner and outer scales respectively. For $\kappa_o << q << \kappa_i$, we obtain the *simple* power-law model: $P_{N_e}(q) = C_{N_e}^2 q^{-\beta}$. Armstrong, Rickett, & Spangler (1995) have constructed an empirical density spectrum by combining radio scintillation observations in the local ISM

($\lesssim 1$ kpc) with measurements of the differential Faraday rotation angles and large-scale electron density gradients. They have shown the power spectrum to be consistent with a simple Kolmogorov power-law model ($\beta = 11/3$) over an astronomical 10 orders of magnitude in wavenumber scale ($10^{-18} \mathrm{m}^{-1} < q < 10^{-8} \mathrm{m}^{-1}$). The Kolmogorov spectrum in density suggests a turbulent cascade in the magnetic and kinetic energies. This has lead to several theoretical investigations of the generation and maintenance of hydromagnetic turbulence in the ISM (e.g. Pouquet, 1978; Higdon 1984 & 1986; Biskamp, 1993: Sridhar & Goldreich 1994; Goldreich & Sridhar 1995 and 1997). However, the Armstrong et al. study combined observations from many lines of sight and the scatter among them leaves a substantial uncertainty in the exponent β. A list of symbols is given in Table 3.

In spite of the positive evidence for the simple Kolmogorov spectrum, substantial observational inconsistencies remain. For instance, long-term refractive intensity scintillations of some pulsars have modulation indices as much as a factor of 2 larger than predicted by the simple Kolmogorov model (cf. Gupta, Rickett, & Coles 1993). Other discrepancies are revealed in the diffractive dynamic spectra of pulsars. On some occasions, periodic fringes are observed, which are not predicted by the simple Kolmogorov model (cf. Roberts & Ables 1982; Cordes & Wolszczan 1986; Rickett, Lyne, & Gupta 1997; Gupta, Bhat & Rao, 1999); in addition, sloping bands in the dynamic spectra often persist longer than predicted by the model (cf. Gupta, Rickett, & Lyne 1994; Bhat, Rao & Gupta, 1999b Bhat, Gupta & Rao, 1999c). Further for some pulsars, the decorrelation bandwidth has larger amplitude variations than predicted for the Kolmogorov spectrum (Bhat, Gupta & Rao, 1999c). Such anomalies suggest the presence of large refractive structures giving rise to the focusing and defocusing of the scattered ray bundles. The interference of the ray bundles can also explain the occasional fringes observed in the dynamic spectra of some pulsars. Given the relatively frequent occurrence of such events, one can ask whether they can be considered as mere occasional anomalies or should be considered as a widespread phenomenon intrinsic to the spectrum on a grand scale.

The observational inconsistencies suggest the need for an enhancement in the power on the large "refractive" (10^{11} m to 10^{12} m) spatial scales relative to the power on the small "diffractive" (10^7 m to 10^8 m)

scales. There are several means by which this ratio may be enhanced. One is to include the inner scale cut-off in the density spectrum, which reduces the power at small scales (Coles et al. 1987); these authors proposed inner scales of $10^8 - 10^9$ m., though this does not correspond to any obvious physical scale. Physically, the inner scale corresponds to the scale at which the turbulent cascade dissipates and becomes a source of heating for the plasma (Spangler, 1991). The value of the inner scale is largely unknown. Using different methods, Spangler & Gwinn (1990), Kaspi & Stinebring (1992), and Gupta et al. (1993) have reported values for the inner scale ranging from 10^4 to 10^9 meters. In proposing the smaller values, Spangler & Gwinn (1990) argued that the inner scale is the larger of the ion inertial length, $L_i \equiv V_A/\Omega_i$ (where V_A is the Alfvén speed, and Ω_i is the ion cyclotron frequency), and the ion Larmor radius, $r_i \equiv v_{th}/\Omega_i$ (where v_{th} is the ion thermal speed); they obtained parameters for the warm ionized medium in reasonable agreement with observations. In a recent discussion, Minter & Spangler (1997) have suggested ion-neutral collisional damping and wave-packet steepening as possible dissipation mechanisms for the turbulence in the diffuse ionized gas, which would make the mean-free path for ion-neutral collisions a possible value for the inner scale. However, this is thought to be larger than the maximum values proposed to explain the observations, making it a less convincing dissipation mechanism. Observationally, the Kolmogorov model with a large inner scale predicts refractive modulation indices consistent with pulsar measurements (Gupta et al. 1993). It has also been proposed to explain the occasional periodic fringes, with an inner scale on the order of the Fresnel scale (Cordes, Pidwerbetsky, & Lovelace 1986; Goodman et al. 1987). However, Rickett et al. (1997) reported a fringe event for the pulsar B0834+06 that could not be explained as the effect of a large inner-scale spectrum. The event requires similar conditions to those needed to explain the extreme scattering events (Fiedler et al. 1987).

Another way to enhance the ratio of the power between the refractive and diffractive scales in the spectrum is to steepen the spectrum—with spectral exponents $\beta > 4$ (Blandford & Narayan 1985; Goodman & Narayan 1985; Romani, Narayan, & Blandford 1986). While power-law spectra with $\beta \sim 11/3$ have a turbulence connotation, spectra with $4 < \beta < 6$ might involve some forms of turbulence, but are also consistent with a distribution of non-turbulent struc-

tures with a range of spatial scales. Such steep spectra with $4 < \beta < 6$ predict refractive modulation indices close to unity (Goodman & Narayan 1985), which is substantially larger than the range 30 to 40 % observed from the nearby pulsars. On this basis Rickett & Lyne (1990) and Armstrong et al. (1995) have rejected spectra steeper than 4 for the interstellar plasma. However, the special case of $\beta = 4$ has been given little attention. We can conceive of a power-law model with spectral exponent $\beta = 4$ given by:

$$P_{N_e}(q; z) = \frac{C_{N_e}^2}{\left(q^2 + \kappa_o^2\right)^2} . \qquad (2)$$

Hereafter, we refer to this model as the "$\beta = 4$ model." Blandford & Narayan (1985) briefly discussed this special case without including a cut-off at low wavenumbers. It is interesting to note that even though the Kolmogorov spectral exponent $\beta = 11/3$ is very close to 4, the $\beta = 4$ model has a very different physical implication. Its physical origin has been rarely discussed, and it has not been formally compared with observations. Physically, this spectrum suggests the random distribution in location and orientation of discrete discontinuous objects across the line of sight. An "outer" scale, $L_o = \kappa_o^{-1}$, is included to account for the typical size of such objects. The "inner" scale here would correspond to the scale of the sharpness of a typical discontinuity. We assume the "inner" scale to be smaller than the diffractive scale of scintillations, and hence has no significant effect on the scintillations. The $\beta = 4$ model could characterize stellar wind boundaries, supernova shock fronts, sharp boundaries of HII regions at the Strömgren radius, or any plasma "cloud" with sufficiently sharp boundaries (transition regions shorter than the diffractive scintillation scale) which may cross the line of sight. Note that, though turbulence is not necessarily implied by the model, strong turbulence which has steepened to form shocks would also be described by the $\beta = 4$ model. In these models a single discrete object crossing the line of sight could also explain the "extreme scattering events" observed in the flux density variations of extra-galactic sources (e.g. Fiedler et al. 1987). We note that the analysis of such events have been primarily based on geometrical optics involving a single "cloud" (Goodman et al. 1987; Cordes et al. 1986; Cordes & Wolszczan 1986; Roberts & Ables 1982; Ewing et al. 1970). Our analysis of the $\beta = 4$ model includes the "wave optics" effects when the line of sight passes through very many

such clouds. The ISM is assumed to consist of a random assembly of discrete structures with abrupt density steps which may be independent of each other. If the $\beta = 4$ model were compatible with all of the scintillation observations, it would remove the implication of interstellar plasma turbulence with an inertial range spanning as much as 10 orders of magnitude in scale, which has become the canonical model for ISS phenomena. It would, however, still be consistent with turbulence that has steepened into shocks.

We start with a simple derivation of the $\beta = 4$ model in section 2. In section 3, we give equations for the wave structure function for the $\beta = 4$ model and compare predictions In section 4, the variation of the diffractive decorrelation bandwidth with frequency is used to test the $\beta = 4$ model against the simple Kolmogorov model and the Kolmogorov model with an inner-scale (hereafter, the "inner-scale" model). In section 5, the observed variation of the refractive scintillation index with the normalized diffractive decorrelation bandwidth is compared with theoretical predictions for the simple Kolmogorov, inner-scale, and $\beta = 4$ models. We use theoretical results from a previous paper (Lambert & Rickett 1999; hereafter, LR99), in which we developed the theory of diffractive scintillations in a medium modeled by these spectra, and we add details of the theory for refractive scintillation in Appendix A. In Appendix B, we discuss the use of the square of the second moment to approximate the intensity correlation function for diffractive scintillation with $\beta = 4$. In section 6 we give a discussion and our conclusions.

2. THE SPECTRUM FOR RANDOM DISCONTINUITIES IN DENSITY

In this section, we give a simple derivation of the $\beta = 4$ model. Consider first a random distribution in space of identical plasma structures (blobs). The resulting electron density may be described as the convolution of a three-dimensional Poisson point process with the density profile of one individual blob. This is the spatial analog of shot noise, in which each charge carrier contributes the same temporal profile of current arriving at randomly distributed times. In the wavenumber domain, the power spectrum of the electron density is then given by the spectrum of the Poisson point process multiplied by the squared magnitude of the Fourier transform of one blob. The spectrum of the Poisson point process is a constant equal

to the number density, n_0, of the blobs in space (Papoulis 1991). Thus the power spectrum of the medium follows the same shape as that of an individual blob. A similar description applies to water droplets in a fog and many naturally occurring media, as discussed by Ratcliffe (1956). If the blobs are asymmetrical and randomly oriented, one must also average the spectrum over the possible angles of orientation.

The basic feature of structures with discontinuous boundaries is that their power spectrum has an asymptotic behavior at large wavenumbers that varies as (wavenumber)$^{-4}$. This is the spatial analog of the idea that the temporal spectrum of any pulse shape with an abrupt rise or fall has a high-frequency asymptote as (frequency)$^{-2}$. The prime example is a rectangular pulse, for which the spectrum is a sinc-squared function, whose high-frequency envelope follows this law. The simplest spatial example is spherical blobs of radius a with uniform density f_0 inside and zero outside; clearly, an added uniform background density does not affect the power spectrum. The three-dimensional spatial Fourier transform of an *isotropic* function $f(r)$ of radial distance r is given by (Tatarskii 1961):

$$F(q) = \frac{1}{2\pi^2 q} \int_0^\infty f(r) \sin(qr) r \, dr \,, \qquad (3)$$

where q is the magnitude of the wavenumber. For any function $f(r)$ that falls to zero beyond a radius a, the integral will vary as $1/q$ in the high-wavenumber limit $qa \gg 1$, making $F(q) \propto 1/q^2$. For the spherical blobs of size a we have:

$$F(q) = \frac{f_0}{2\pi^2 q} \left\{ -\frac{a \cos(qa)}{q} + \frac{\sin(qa)}{q^2} \right\} \,. \qquad (4)$$

For the squared magnitude of the Fourier transform, for very small and large values of qa:

$$|F(q)|^2 = \begin{cases} f_0^2 a^6 / (36\pi^4) \,, & qa << 1 \,, \\ \\ q^{-4} \, a^2 f_0^2 / (8\pi^4) \,, & qa >> 1 \,. \end{cases} \qquad (5)$$

The spectrum of the electron density is then $n_0 |F(q)|^2$. We can approximate this by equation (2), which exactly matches equation (5) at small and large values of qa, with $C_{N_e}^2 = n_0 a^2 f_0^2 / (8\pi^4)$ and $\kappa_o^{-1} = L_o = (2/9)^{0.25} a$.

There are evident generalizations to make the model more like a real medium. The spheres could have a

probability distribution for their radii, which would weight the average of the square of equation (4). The spheres could have smoothly varying density inside and an abrupt boundary at radius a. As with the pulse example, the high-wavenumber behavior would not change. More realistic models would include anisotropic structures with random orientations and a distribution of scales. For example, consider a circular cylinder as a model for an anisotropic blob, with a particular radius and thickness. Its Fourier transform can be computed with respect to its major axes. This can then be transformed to tilted axes and the result averaged over an isotropic distribution of angles of tilt. Evidently the result will also be isotropic; we have solved this approximately and find a spectrum with the same high-wavenumber *asymptotic* form as equation (2), where the "outer scale," L_o, is the smaller of the thickness and radius. This result could be averaged over a probability distribution of radii and thicknesses and a similar conclusion reached, with L_o as a weighted average of the smallest dimension. Planar sheets at random angles are modeled as very flat cylinders and provide a crude representation of a distribution of shocks. Another simplified model would be ellipsoids of different sizes, eccentricities, and orientations, and again we expect a similar result.

We conclude that the $\beta = 4$ spectrum is an approximate description of the power spectrum for a medium with a random distribution of discontinuous structures, in the limit for wavenumbers greater than the reciprocal of the smallest dimension across the structures. We note that for wavenumbers at or below about $\kappa_o = L_o^{-1}$ the functional form depends on the detailed shapes, though it will be much less steep than κ^{-4}. Thus equation (2) will not be generally applicable at the lowest wavenumbers. Similarly, in practice there is a finite scale over which the density jump occurs (e.g. shock thickness). This can be modeled by convolving the idealized discontinuous structures with a suitable narrow, say, Gaussian function which thus provides a very high-wavenumber cut-off beyond which the spectrum falls rapidly to zero. Consequently, we consider a spectrum with an inverse fourth power law between inner and outer scales, though these do not have the same connotations as inner and outer scales in a turbulent cascade. We do not discuss the physical origin of the supposed discontinuous plasma structures beyond the ideas formulated in the Introduction, such as supernova shock

fronts, stellar wind boundaries or sharp boundaries of HII regions at the Strömgren radius. There needs to be no physical coupling between the individual blob structures, and there is no turbulent cascade implied by the $\beta = 4$ spectrum. However, we note that shocks developing from the steepening of very strong turbulence could also be described by the model, and so if successful, the model would not rule out such strong turbulence, though in this case the $\beta = 4$ range does not correspond to an inertial cascade as does the $11/3$ spectrum.

In the following sections, we give the necessary scintillation theory needed to develop equations for the scintillation observables corresponding to the $\beta = 4$ model, which we then compare with ISS observations. We concentrate on measurements which are sensitive to the form of the density spectrum and are relatively insensitive to the distribution of scattering material along the line of sight.

3. PHASE STRUCTURE FUNCTION

Central to the description of the second moment and the coherence function for intensity is the phase structure function. The longitudinal gradient of the phase structure function is related to the electron density spectrum through (cf. Coles et al. 1987):

$$
\begin{aligned}
D'_\phi(s, z; \nu) \;=\; & \frac{8\pi^2 r_{\rm e}^2 c^2}{\nu^2} \int_0^\infty P_{N_e}(\kappa, q_z = 0; z) \\
& \times \left[1 - J_0(\kappa s) \right] \kappa \, d\kappa \,.
\end{aligned} \tag{6}
$$

Here c is the speed of light, $r_{\rm e}$ is the classical electron radius, and ν is the radio frequency. For a plane wave incident on a scattering medium, the line of sight integral of $D'_\phi(s, z; \nu)$ gives the structure function of the geometric optics phase, also called the *wave* structure function, $D_\phi(s)$. For the spherical wave geometry applicable to a pulsar at distance L, the separation s at the observer's plane is projected back to the point of integration, giving $D_{\rm S}(s) = \int_0^L D'_\phi(sz/L, z; \nu) \, dz$. The integrals are evaluated explicitly in equations (13), (17), and (21) of LR99 for a uniform scattering medium with the simple power-law, inner-scale, and $\beta = 4$ spectral models, respectively. In the extended scattering geometry, the field coherence length at the observer, s_0, is defined by: $D_{\rm S}(s_0) = 1$. For a screen of thickness Δz at distance z_p from the pulsar, the wave structure function at the observer becomes $D_{\rm S}(s) = D'_\phi(s z_p/L, z_p; \nu) \Delta z$, which has an explicit dependence on the screen location. In

LR99, we found it useful to define a coherence scale $s_{0,\text{scr}}$ for the screen by its phase structure function $D_\phi(s_{0,\text{scr}}) = D'_\phi(s_{0,\text{scr}}, z_p; \nu)\Delta z = 1$, which is independent of the screen location. Note that in applying equation (6), we are assuming that the screen thickness, Δz, is much greater than the outer scale L_o and small compared to total distance L.

Here, we repeat the equation for the phase structure function of the $\beta = 4$ model in a thin layer (screen). Substituting the $\beta = 4$ model for the density spectrum into equation (6), integrating, and multiplying by the screen thickness, Δz, we obtain:

$$D_\phi(s) = \frac{4\pi^2 r_\text{e}^2 c^2 SM}{\kappa_o^2 \nu^2} \left[1 - (\kappa_o s)K_1(\kappa_o s)\right] , \qquad (7)$$

where K_1 is the first order modified Bessel function of the second kind, and $SM = C_{N_e}^2 \Delta z$ is the scattering measure. Equation (7) may be approximated by the following logarithmic expression:

$$D_\phi(s) = \frac{\pi^2 r_\text{e}^2 c^2 SM}{\nu^2} s^2 \ln\left[1 + \frac{4}{(\kappa_o s)^2}\right] , \qquad (8)$$

which matches the full Bessel expression at both large and small values of the argument. The detailed shape, near where the structure function flattens, is governed by the shape of the low-frequency turnover in our model spectrum, equation (2); however, as noted above, the turnover shape depends on details of the density profiles in the plasma blobs which are not constrained in our density model.

The logarithmic structure function for the $\beta = 4$ model has far-reaching consequences. As the outer scale becomes larger, the structure function approaches a square-law. However, due to the presence of the logarithm, this occurs only slowly; that is, only at the limit as s goes to zero does the $\beta = 4$ model structure function become exactly square-law. A square-law structure function for the medium is a convenient mathematical model, but as noted in LR99, in a real medium the structure function must eventually saturate at very large separations. Nevertheless, the square-law structure function has been widely used since it provides a valid approximation for scales smaller than the reciprocal of the wavenumber at which the spectrum is cut-off. The fact that the $\beta = 4$ model structure function deviates from a pure square-law, even for very large values of the outer scale, makes this model interesting and an independent investigation worthwhile.
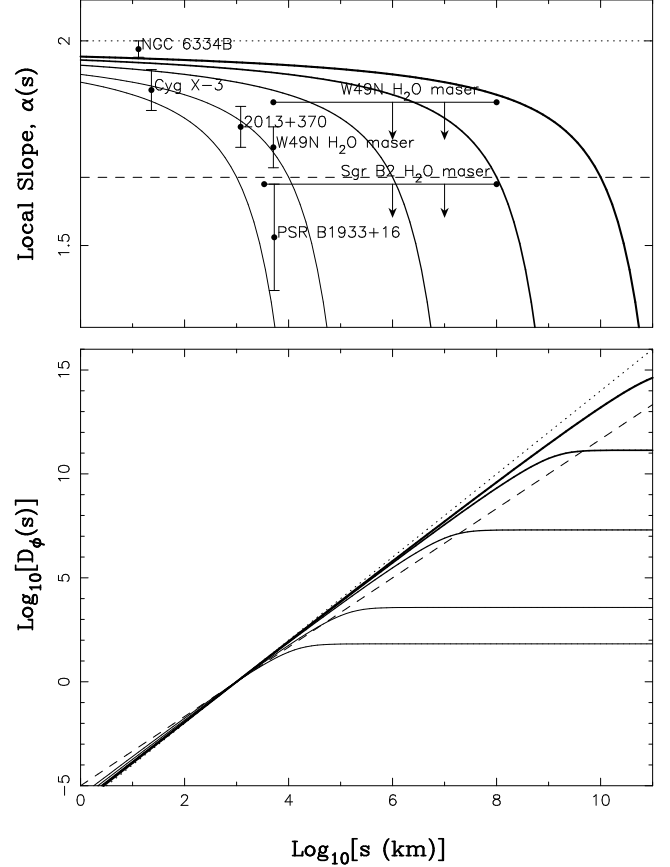

Fig. 1.— Local logarithmic slope, $\alpha(s)$, of the phase structure function (upper panel) and the phase structure function (lower panel) for the $\beta = 4$ model. We have set $s_0 = 1000$ km for all curves, and the solid lines correspond to different values of the outer scale, L_o. In going from the thinnest to thickest solid lines, the outer scales are: 10^4, 10^5, 10^7, 10^9, and 10^{11} km, respectively. The thin dashed line corresponds to the simple Kolmogorov model with logarithmic slope of $5/3$, and the thin dotted line corresponds to the square-law structure function. The points in the upper panel correspond to measured local logarithmic slopes of the phase structure function obtained from VLBI (Spangler & Gwinn 1990).

6

In Figure 1, we have plotted the structure function of the $\beta = 4$ model and its effective local logarithmic slope, $\alpha(s)$, versus the transverse spatial lag, s, for various values of the outer scale, L_o (see equation 20 of LR99). To illustrate the shapes, we have chosen $s_{0,\text{scr}} = 1000$ km for all curves. The thin dashed lines correspond to the simple Kolmogorov model with logarithmic slope of $5/3$, and the thin dotted lines correspond to the square-law structure function. The plot shows how slowly the local slope approaches 2; even for $s/L_o \sim 10^{-8}$, the slope is 1.95–distinctly less than 2.

The points in the upper panel correspond to measured local exponent of the wave structure function obtained from VLBI observations, as tabulated by Spangler & Gwinn (1990). In principle, this method of comparison provides a good test for the form of the density spectrum. These authors presented a similar plot corresponding to the inner-scale model, for which $\alpha(s)$ is close to 2.0 for s less than the inner scale and close to $5/3$ for s greater than the inner scale, with a transition occurring over about a decade in s. They derived estimates of the inner scale ranging from 50,000 to 200,000 meters, for the highly scattered sources that they studied. Whereas there is some uncertainty in some of the estimates of α, there are several examples in which values greater than $5/3$ are reliably observed (e.g. Trotter et al., 1998). As can be seen, there is also reasonable agreement with the $\beta = 4$ model. Assuming the model to be correct, a separate model-fitting to each observation yields an outer scale in the range $L_o \sim 3 \times 10^7$ to 10^8 meters. These values are much smaller than the parsec scales of supernova remnants and interstellar clouds. However based on this comparison alone, we are unable to discriminate between the inner-scale and $\beta = 4$ models since they both provide equally satisfactory agreement with the observations. Hence further independent tests are needed, and in the following sections, we present comparisons with two other scintillation observables which in the end argue against the $\beta = 4$ model as a universal description of the ionized ISM.

4. DIFFRACTIVE DECORRELATION BANDWIDTH

The diffractive decorrelation bandwidth, $\Delta\nu_d$, is perhaps the easiest ISS observable to measure. It is the frequency-difference for a decorrelation to 50% of the correlation function for diffractive intensity scintillations. These are usually recorded as a dynamic spectrum centered on a given radio frequency, ν, for a pulsar. Observations of $\Delta\nu_d$ for one pulsar at a wide range of radio frequencies have provided an important test of power-law models for the interstellar density spectrum on that particular line of sight. When the diffractive scale is far from the inner and outer scales, one expects $\Delta\nu_d \propto \nu^{2\beta/(\beta-2)}$, which for the simple Kolmogorov model is $\nu^{4.4}$, in both screen and extended medium geometries. In this section we re-examine the published measurements and compare them with theory for the three different spectral models. Since the scaling laws are all so steep, in Figures 2 and 3, we have plotted the observations logarithmically as $\Delta\nu_d/\nu^4$. Overplotted are lines giving the theoretical predictions for our three spectral models, with the simple Kolmogorov model as a line of slope 0.4. Before giving our conclusions, we must discuss the error bars and various corrections to the data and also the method for deriving the theoretical predictions.

Observations

Decorrelation bandwidth data, collected together by Cordes, Weisberg, & Boriakoff (1985; hereafter, CWB), for pulsars PSR B0833$-$45 (Vela), PSR B0329-+54, PSR B1642$-$03, PSR B1749$-$28, and PSR B1933+16 are shown in Figures 2 and 3. We have also included recently measured points by Johnston et al. (1998) for the Vela pulsar. These are $(\nu, \Delta\nu_d) = (8.4\,\text{GHz}, 13.9\,\text{MHz})$ and $(13.7\,\text{GHz}, 58.2\,\text{MHz})$. The data are shown as solid circles if derived from dynamic spectra and as solid stars if derived from pulse broadening measurements. The latter become easier to estimate at low frequencies, where the resolution bandwidth required for the former becomes too narrow for an adequate signal-to-noise ratio. The conversion of an estimate of a pulse broadening time to a decorrelation bandwidth relies on the uncertainty relation $2\pi\Delta\nu_d\tau_d = C_1$. Unfortunately, the "constant" C_1 takes on different values for different geometries and spectral models. For the $\beta = 4$ model, it is also very weakly dependent on frequency. In Table 1 of LR99, we gave numerical values for C_1 for the three spectral models with spherical waves in both a screen and an extended medium geometry. For a given geometry, the smallest C_1 is for the Kolmogorov spectrum and the largest (by about 50%) is for the square-law structure function. Thus in Figures 2 and 3 we plot, as solid and open stars, the values converted using
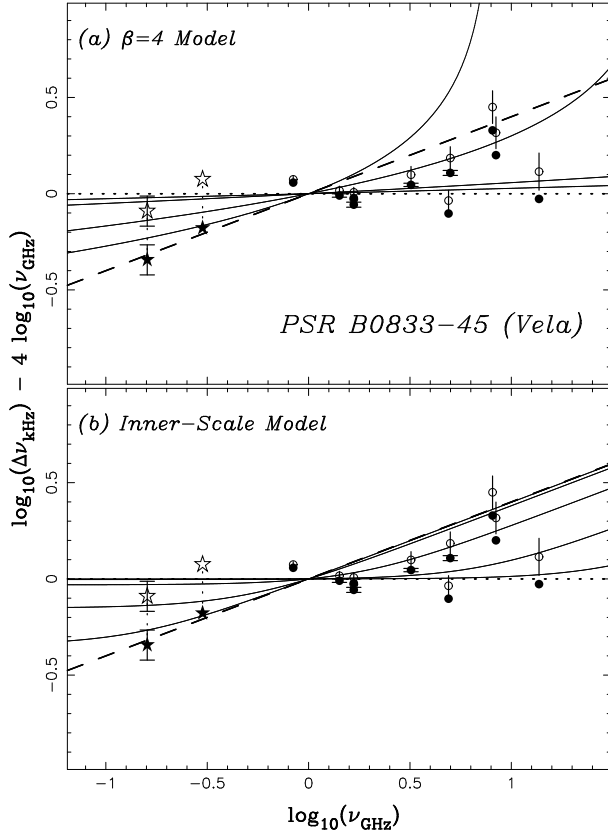
Fig. 2.— Diffractive Decorrelation bandwidth versus
frequency for PSR B0833−45 (Vela). For visual aid,
a line of slope 4 has been subtracted from the log/log
plots so that the frequency scaling for the square-law
structure function model, indicated by the thick dot-
ted line, would coincide with the abscissa. The filled
stars correspond to decorrelation bandwidths com-
puted from scattering broadening times using the Kol-
mogorov value for the constant C_1, whereas the open
stars correspond to the C_1 from square-law structure
function model. All lines are computed for the ex-
tended medium, but would be nearly the same for a
screen geometry. The thick dashed line corresponds
to the simple Kolmogorov model. For the $\beta = 4$
model (a), 4 solid lines have been drawn correspond-
ing to parameter $\kappa_o s_{0,1\mathrm{GHz}}$ equal to 10^{-16} (line clos-
est to the square-law structure function model), 10^{-8},
10^{-3}, and 10^{-1} (line flaring furthest from the simple
Kolmogorov curve). For the inner-scale model (b), 5
solid lines have been drawn for parameter $\kappa_i s_{0,1\mathrm{GHz}}$,
ranging from 10^{-1} (line closest to the square-law
structure function model) to $10^{1.5}$ (line closest to
the simple Kolmogorov model), in equal logarithmic
steps.

C_1 for the Kolmogorov and square-law structure func-
tion models, respectively. We display the predictions
for extended medium and note that the screen values
are only about 20% less for each spectrum. Thus in
comparing data with the theory for the $\beta = 4$ and
inner-scale models, the data should lie between the
extremes of the open and solid stars, depending on
the outer and inner scales, respectively. Note that
the value of C_1 in equation (7) of the Taylor et al.
(1993) catalog is more than 50% greater than values
computed by LR99, since it concerns the mean pulse
delay rather than the $1/e$ decay time of the pulse.

The second correction to the data concerns the ef-
fects of refractive scintillation at the higher radio fre-
quencies, which are closer to the transition to weak
scintillation. Gupta et al. (1994) gave a heuristic
theory of the effect and expressions for the bias to
the diffractive $\Delta\nu_d$ due to refractive shifts; LR99 dis-
cussed the effect from the work of Codona et al. (1986;
hereafter, CCFFH). In Figures 2 and 3, we have plot-
ted as open circles $\Delta\nu_d$ corrected for this effect using
equation (D6) of Gupta et al. (1994), who also esti-
mated the variability in estimates of $\Delta\nu_d$ due to the
refractive modulation. We used this to estimate an
error bar on the open circles, which is typically larger
than the error bars quoted by the original observers,
plotted on the solid circles.

In summary, the open circles and their error bars
provide the best direct estimates of $\Delta\nu_d$ and the in-
direct estimates lie between the open and solid stars.

Theory

The theory of diffractive scintillations has been dis-
cussed by many authors; we will use the results of
section 6 in LR99 for a point source (spherical waves)
either in an extended scattering medium or with a
screen at z_p from the pulsar and z_o from the ob-
server (with $z_p + z_o = L$). Following usual practice,
we assume the strong scattering limit, in which the
frequency decorrelation function for intensity is the
squared magnitude of the diffractive component of the
two-frequency second moment of the field. The valid-
ity of this approximation is examined in Appendix B,
where we find that it introduces a small error for the
$\beta = 4$ model, which however is negligible compared
to the errors in the observations. The decorrelation
bandwidth, $\Delta\nu_d$, can be defined in terms of a normal-
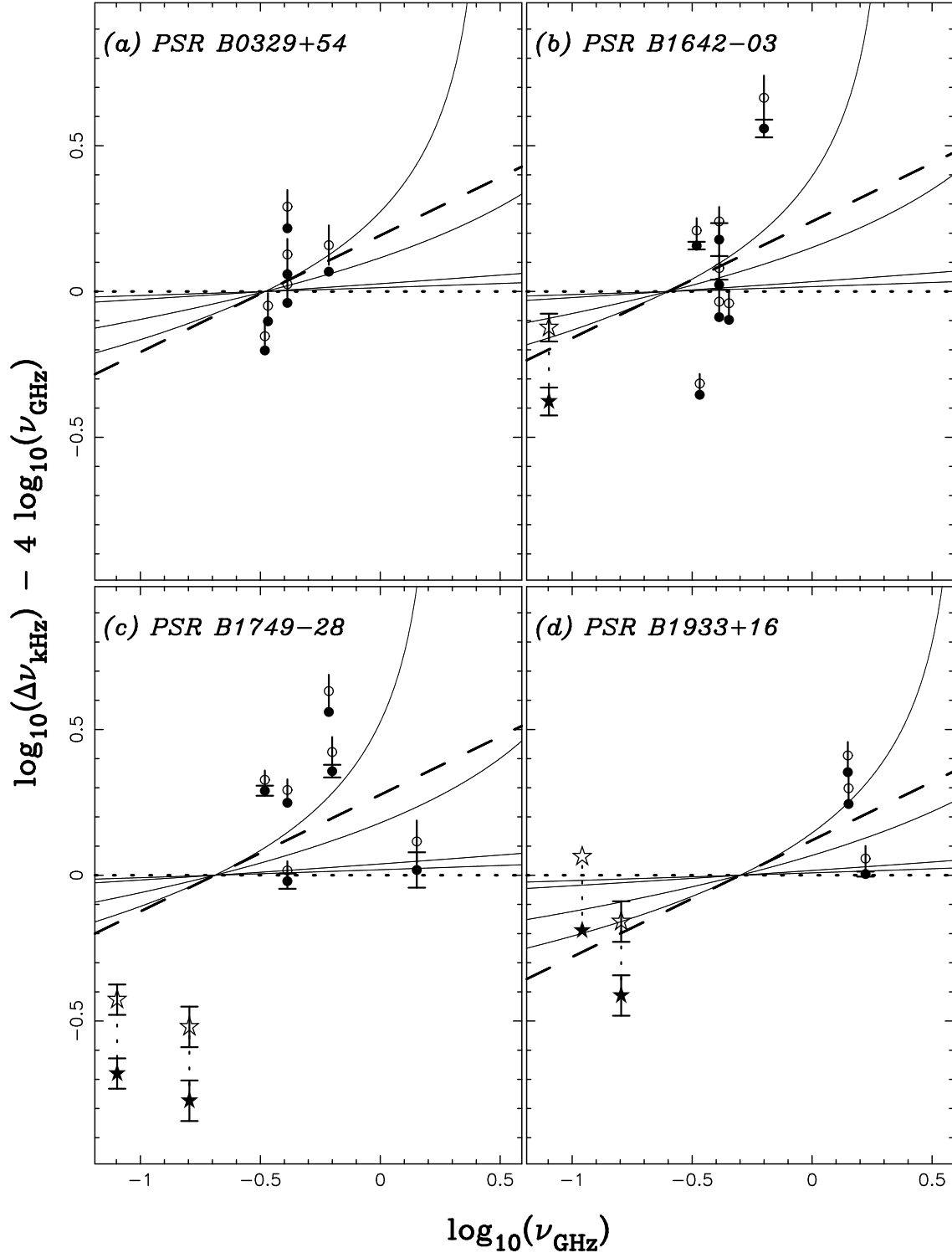
Fig. 3.— Diffractive Decorrelation bandwidth versus frequency for 4 pulsars plotted as for Figure 2. Only theoretical curves for the $\beta = 4$, simple Kolmogorov, and square-law structure function models are shown.

ized bandwidth, v_d:

$$\Delta\nu_d = \frac{v_d \nu}{u^2} \quad \text{where} \quad u^2 = \frac{z_{\text{scatt}} c}{2\pi\nu s_0^2} \ . \qquad (9)$$

Here ν is the (geometric) mean of the two frequencies, and the parameter u determines the strength of scattering; c is the speed of light and z_{scatt} is the effective scattering distance. For a uniform scattering medium, $z_{\text{scatt}} = L$, and for a screen geometry, $z_{\text{scatt}} = z_e = z_o z_p/L$. s_0 is the field coherence scale where the appropriate phase structure function equals unity; for the uniform scattering medium, it is defined at the observer, and for a screen, it is $s_{0,\text{scr}}$ which is independent of the distances to the pulsar and screen, and leads to u_{scr} as the appropriate strength of scattering parameter.

The computations presented in LR99 include a tabulation of the normalized bandwidth v_d for the various models under discussion, and associated plots of the intensity decorrelation function itself. For the simple Kolmogorov model, a constant value for v_d is obtained regardless of the frequency or distance (0.773 and 0.654 for the extended medium and screen geometries, respectively). Thus the frequency dependence of $\Delta\nu_d$ reflects the frequency dependence of s_0, giving $\Delta\nu_d \propto \nu^{2\beta/(\beta-2)}$. CWB used this to estimate β from observations of $\Delta\nu_d$. We now compare the observations with theoretical scaling laws for the two other spectral models. There are, however, some complications. The quantity v_d is no longer exactly independent of frequency, and s_0 depends on both frequency and the outer scale, L_0, or the inner scale, L_i, that parameterize the other two models.

Consider the details for the discontinuity spectrum. In Figure 2, we plot $\Delta\nu_d/\nu_{\text{GHz}}^4$ versus ν_{GHz} as observed for the Vela pulsar. In Figure 2a, we have plotted theoretical curves for $\beta = 4$ model with various outer scales. We use equation (9) for the models and so need the variation of both s_0 and v_d with ν.

For a screen, we determine $s_{0,\text{scr}}$ from equation (8) for the $\beta = 4$ model, and eliminate the scattering measure SM using the same equation for $s_{0,1\text{GHz}}$ at a reference frequency of 1 GHz. This gives a relation between $s_{0,\text{scr}}/s_{0,1\text{GHz}}$ and ν_{GHz}, with $L_o/s_{0,1\text{GHz}}$ as a parameter. For an extended scattering medium, we use equation (21) of LR99 to determine s_0 at the observer, and the same method as for the screen to eliminate SM. In Figure 4, we show the variation of v_d with L_o/s_0 at a fixed frequency (computed by Lambert 1998 and described in LR99). This is combined

with the s_0–ν_{GHz} relation to obtain the relation of v_d to ν_{GHz}. For the curves in Figure 2, $s_{0,1\text{GHz}}$ is determined so that, for each value of L_o, the model $\Delta\nu_d$ fits the measured values near 1GHz. For most of the models of interest $L_o \gg s_0$, and then the logarithm functions vary much more slowly than the s_0^2 term in equation (8). In which case there is nearly a linear relation $s_0/s_{0,\text{ref}} = \nu/\nu_{\text{ref}}$. Furthermore, Figure 4 shows that as s_0 changes, the parameter v_d changes very slowly. Consequently, for a very wide range of the outer scale, a good approximation is $\Delta\nu_d \propto \nu^4$, which reflects the fact that the underlying structure function then approaches a square-law behavior.

Consider the plot for the Vela pulsar PSR B0833−45 (Figure 2) for which the data are most extensive. Although we have computed curves and data corrections for both the screen and extended scattering geometries, we only show the extended medium results in Figure 2 because the two plots are so similar. In the comparison with the screen model, the star points are lowered about 0.08 vertical units (20%), and the $\beta = 4$ model curves are very slightly steeper functions of frequency. However, the scatter among the observations is greater than the differences in the models between screen and extended geometries. In the Vela plot, we see that the $\beta = 4$ model agrees somewhat better with the observations than does the simple Kolmogorov model. This pulsar is known to lie in a highly scattered region, and hence the presence of discontinuities, as incorporated in the $\beta = 4$ model, is perhaps reasonable. However, the conclusion is not strong, since the data are also reasonably fitted by an inner scale in the range 100 km to 500 km, as can be found from Figure 2b.

For the other pulsars (Figure 3), the data show a stronger frequency dependence than predicted by both the simple Kolmogorov and $\beta = 4$ models. However, the inconsistencies between the measurements at different frequencies are even greater, and better observations are needed, before such comparisons could discriminate between the models. A recent series of measurements at 327 MHz (Bhat et al. 1999a,b,c) documents the variability of $\Delta\nu_d$, and a similar long sequence of such measurements at other frequencies is needed on the same pulsars, before reliable conclusions can be reached from the frequency scaling observations.
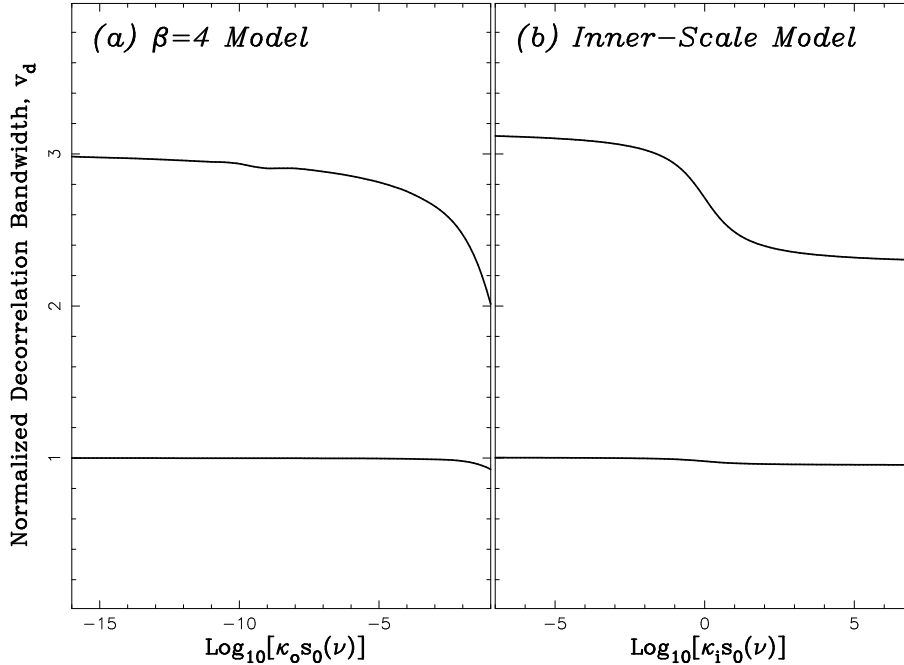
Fig. 4.— Variation of the normalized diffractive decorrelation bandwidth, v_d. (a) The $\beta = 4$ model, upper curve for an extended medium geometry with parameter $\kappa_o s_0$ and lower curve for a screen geometry versus $\kappa_o s_{0,\mathrm{scr}}$. (b) Same plots for the inner-scale model.

5. REFRACTIVE SCINTILLATION INDEX

Slow variations in the flux of pulsars are caused by refractive interstellar scintillation (RISS), and can be characterized by the rms deviation in flux density normalized by its mean, or scintillation index, m_R. RISS is due to inhomogeneities in the interstellar electron density on scales much larger than those responsible for diffractive scintillation, as characterized by the decorrelation bandwidth. There are now measurements of both phenomena on a substantial number of pulsars, from which we can constrain the density spectrum on each line of sight. The relation of the refractive scintillation index, m_R, to the normalized diffractive decorrelation bandwidth, $\Delta\nu_d/\nu$, depends on the ratio of the power in the density spectrum at the large refractive scales (10^{11} m to 10^{12} m) to the power at the smaller diffractive scales (10^7 m to 10^8 m).

We compare pulsar measurements gathered from the literature with theoretical predictions by plotting m_R versus $\Delta\nu_d/\nu$ (cf. Rickett & Lyne 1990 and Gupta et al. 1993). Related tests have been made by Armstrong et al. (1995), Bhat et al. (1999a) and Smirnova, Shishov, & Stinebring (1998). m_R measurements at

610 MHz are listed in Table 1 and include the results of long-term monitoring observations by Smirnova et al. (1998), and older measurements near 100 MHz are listed in Table 2. The tables also include the decorrelation bandwidth obtained from diffractive scintillation, typically observed at a different radio frequency, scaled to the observing frequency for m_R. We used the Kolmogorov scaling law $\Delta\nu_d \propto \nu^{4.4}$, and we note that the minor differences that result from changes in the scaling law for other spectral models are insignificant in the comparison. The 100 MHz data consist of m_R measurements at 73.8 MHz, 81.5 MHz, and 156 MHz. The pulsars observed at 610 MHz are primarily located at distances $\gtrsim 1$ kpc, whereas the pulsars observed at 100 MHz are nearer at distances $\lesssim 1$ kpc. Figures 5 and 6 show plots of the theoretical and measured refractive scintillation index versus the normalized decorrelation bandwidth in separate panels for the two sets of measurements. Theoretical curves are also shown in the Figures for different spectral models in both the screen and extended medium geometries. The dashed line corresponds to the simple Kolmogorov model ($\alpha = 5/3$), and the solid lines in Figures 5 and 6 correspond to the $\beta = 4$ and inner-scale models, respectively.

11

In section 4 we noted that variable refraction tends to decrease the measured decorrelation bandwidth and used an expression from Gupta et al. (1994) to apply a nominal correction to measured values. In the table of data from near 100 MHz, we have made use of the recently published measurements of Bhat et al. (1999a). They monitored the apparent decorrelation bandwidth near 327 MHz for 20 nearby pulsars, many of which have m_R measurements in Table 2. They found the bandwidth to vary by factors 3-5 and discussed the influence of varying refraction as a refractive bias. From their measurements, they derived a corrected decorrelation bandwidth, which we have scaled (using the $\nu^{4.4}$ scaling law) to the frequency at which m_R was observed. These gave values typically 2–5 times bigger than obtained from earlier measurements (e.g. Cordes 1986). The pulsar B0809+74 was not observed by Bhat et al. (1999a); however, the recent weak scintillation observations of this pulsar by Rickett et al. (1999) similarly suggests that earlier decorrelation bandwidth measurements overestimated the strength of scattering. The effect of these changes is to shift the plots to the right in Figures 5 and 6 by about half a decade, compared to Figure 5 of Gupta et al. (1993). There is only one pulsar (B0329+54) in Table 1 common to the Bhat et al. (1999a) observations, and its decorrelation bandwidth has also been corrected for the refractive bias. Since the pulsars observed at 610 MHz were mostly more heavily scattered, the refractive bias correction is substantially smaller (see Gupta et al. 1994) and has been ignored.

Theory

The theory of refractive scintillations has been known since the 1970s and was applied to pulsar flux variations by Rickett et al. (1984). For example, Prokhorov et al. (1975) described how the modulation index for intensity can exceed unity in strong scattering in their equations (4.53) *et. seq.* We use the notation of Coles et al. (1987) and confine our discussion to spherical wave sources, propagating in a scattering plasma which is either concentrated in a screen or extended uniformly between source and observer. The "low-frequency" approximation for the intensity covariance function is given by equation (10) of Coles et al. (1987), from which we obtain the normalized refractive variance, m_R^2, by setting the spatial

offset equal to zero:

$$
\begin{aligned}
m_R^2 &= \frac{16\pi^2 r_e^2 c^2 L}{\nu^2} \int_0^1 \int_0^\infty P_{N_e}(\kappa, q_z = 0; z) \times \\
&\quad \exp\left\{-L \int_0^1 D'_\phi \left[\kappa r_{F,L}^2 h(x,y)\right] dy\right\} \times \\
&\quad \sin^2\left[0.5\kappa^2 r_{F,L}^2 x(1-x)\right] \kappa d\kappa\, dx, \quad (10)
\end{aligned}
$$

where:

$$
\begin{aligned}
h(x,y) &= \min\left[y(1-x), x(1-y)\right] \quad (11) \\
r_{F,L} &= \sqrt{Lc/2\pi\nu}.
\end{aligned}
$$

Here the transverse wavenumber is $\kappa = \sqrt{q_x^2 + q_y^2}$, and $x = z/L$, where z is the distance along the line of sight measured from the source. For the screen geometry, both the density spectrum and the gradient in the phase structure function D'_ϕ are concentrated in a thin layer of thickness Δz at distance z_p from the source and z_o from the observer. Thus the x and y integrations in equation (10) give $x = y = z_p/L$, and we find it useful to define an equivalent Fresnel scale $r_{F,scr}$:

$$
r_{F,scr} = \sqrt{z_e c/2\pi\nu} \quad \text{where} \quad z_e = z_p z_o/L. \quad (12)
$$

The κ integration in equation (10) involves the product of the density spectrum, decreasing as a steep power of κ, times the high-pass Fresnel filter $\propto \kappa^4$ up to $r_{F,scr}^{-1}$, times the low-pass exponential term that cuts off wavenumbers above s_R^{-1}, where $s_R = u_{scr} r_{F,scr}$ is the radius of the scattering disc. Hence in strong scattering ($u_{scr} > 1$) we only consider the κ^4 part of the Fresnel filter. Consequently, the integration depends on the ratio L_o/s_R or L_i/s_R. For an extended scattering medium the line-of-sight integration softens the exponential cut-off in the κ integration, but the basic relationships remain the same. As others have noted the level of refractive scintillation is greater in an extended medium than in a screen with the same observed diffractive scintillation.

The canonical spectral model in ISS studies of pulsars has been the simple Kolmogorov spectrum $P_{N_e}(q,z) = C_{N_e}^2(z) q^{-11/3}$. By fitting this model to diffractive scintillation observations, observers have estimated the scattering measure, $SM = \int_0^L C_{N_e}^2(z) dz$, toward many pulsars. When divided by the pulsar distance, this gives a line-of-sight average of $C_{N_e}^2(z)$, which is found to vary greatly from one direction to

another and to increase dramatically for distant pulsars seen at low galactic latitudes (e.g. CWB). Taylor & Cordes (1993) have developed a smoothed model for the Galactic plasma density distribution, which includes enhanced scattering in spiral arms and toward the Galactic center. However, there are also large random variations on much finer spatial scales, which would produce a scatter in a plot of m_R against distance of dispersion measure. For a simple power-law spectrum both m_R and $\Delta\nu_d/\nu$ depend on SM through a single strength of scattering parameter. Thus for the Kolmogorov spectrum the variation of m_R with $\Delta\nu_d/\nu$ is independent of distance or frequency and is given by a single dashed line in each plot in Figures 5 and 6. If the scattering medium is uniform, the strength of scattering is $u = r_{\mathrm{F},L}/s_0$. For the screen it becomes $u_{\mathrm{scr}} = r_{\mathrm{F,scr}}/s_{0,\mathrm{scr}}$, and in that case, the dashed theoretical line is independent of the location of the screen between the source and the observer. This point is substantiated in Appendix A, where the theory is laid out in more detail. According to this screen model, along each line of sight there is a scattering layer with a certain SM, which determines both m_R and $\Delta\nu_d/\nu$, but SM is not necessarily related to the pulsar distance. The theoretical curve with SM as the variable is independent of where the layer is located along the line of sight.

For the $\beta = 4$ and inner-scale models, the theoretical curves for m_R versus $\Delta\nu_d/\nu$ depend on the extra parameter L_o or L_i, respectively. Details of the theory are given in Appendix A, where the relevant parameters are shown to be $L_o/s_{0,\mathrm{scr}}$ and $L_i/s_{0,\mathrm{scr}}$. Since $s_{0,\mathrm{scr}}$ depends on frequency, SM, and distance, then m_R also depends somewhat on frequency and distance. In order to fix the frequency dependence of the theoretical m_R values, we have separated the measurements into two groups (at 610 MHz and near 100 MHz). The distance dependence is dealt with by assuming that $SM \propto$ distance. Whereas this is clearly appropriate for the extended scattering medium, it is less clear for the screen model, since the screen model supposes that SM is not necessarily related to distance. However, it is reasonable that, if on a long line of sight there is a single region that dominates the scattering, its SM value will statistically increase with line-of-sight distance. Indeed the experimentally derived scattering measure increases faster with distance than if the medium were uniform (see Figure 1 of Cordes et al. (1991).

In Figure 5 we show the theoretical curves for m_R

in the $\beta = 4$ model, which are relatively flat where $L_o > s_R$. As u increases ($\Delta\nu_d/\nu$ decreases), s_R increases, and when $s_R > L_o$ the scintillations are suppressed. In a screen this occurs when $\Delta\nu_d/\nu \lesssim (r_{\mathrm{F,scr}}/L_o)^2$.

Inspection of Figure 5 shows that the measured m_R values at 100 MHz are above the prediction of the simple Kolmogorov model for the extended medium geometry. These measurements can, however, be modeled with the $\beta = 4$ spectrum with suitable specific choices of outer scale, L_o. The screen geometry is inconsistent with the measurements at 100 MHz for both the simple Kolmogorov and $\beta = 4$ models. For the 610 MHz data, the measured m_R values are mostly in agreement with the prediction of the simple Kolmogorov model for the extended medium geometry; however, they lie below the predictions of the $\beta = 4$ model. For the screen geometry, the measured m_R values are above the simple Kolmogorov model curve. However, for the $\beta = 4$ model, though less convincingly, an agreement with the measurements can be found by suitable choices of the outer scale, L_o. The most striking feature of the Figure is the good agreement with the uniform extended Kolmogorov model for most of the pulsars. This result, relies most heavily on the excellent data from Smirnova et al. (1998), who also note this agreement. We are persuaded by this Figure that the $\beta = 4$ model cannot be viewed as a global alternative to the Kolmogorov spectrum. We also conclude that for the medium-distance pulsars measured at 610 MHz, m_R does not agree with the screen geometry. It appears that even if the scattering medium is not uniform on scales of a few kpc, there is not a single region that dominates the scattering. Computations of m_R due to a patchy distribution along the line of sight could test what distribution would start to approximate the uniformly extended medium.

Turning to a comparison with the alternative inner-scale spectrum in Figure 6, the 100 MHz observations could be explained by very large values of L_i (10^{10}m to 10^{11}m) in a screen configuration or by more modest, but still large, values of L_i (10^8m) in an extended medium. The latter was essentially the proposal made by Coles et al. (1987) for the nearby lines of sight. The 610 MHz points are relatively lower than those at 100 MHz. For an inner scale spectrum in a screen, large values of L_i (10^8m to 10^{10}m) would be necessary; and in an extended medium 60% of the points lie near the simple Kolmogorov model, with the rest

Fig. 5.— Theoretical and measured refractive scintillation indices, m_R, versus the normalized diffractive decorrelation bandwidth, $\Delta\nu_d/\nu$. (a) and (b) show measurements at 610 MHz; (c) and (d) correspond to measurements near 100 MHz. The solid curves give the theoretical results for the $\beta = 4$ model with a range of outer scales from 10^{10} m to 10^{16} m, going from right to left in equal logarithmic steps. The dashed line corresponds to the simple Kolmogorov model in the strong scattering limit. Panels (a) and (c) give theory for a screen geometry; panels (b) and (d) for a uniform scattering medium.
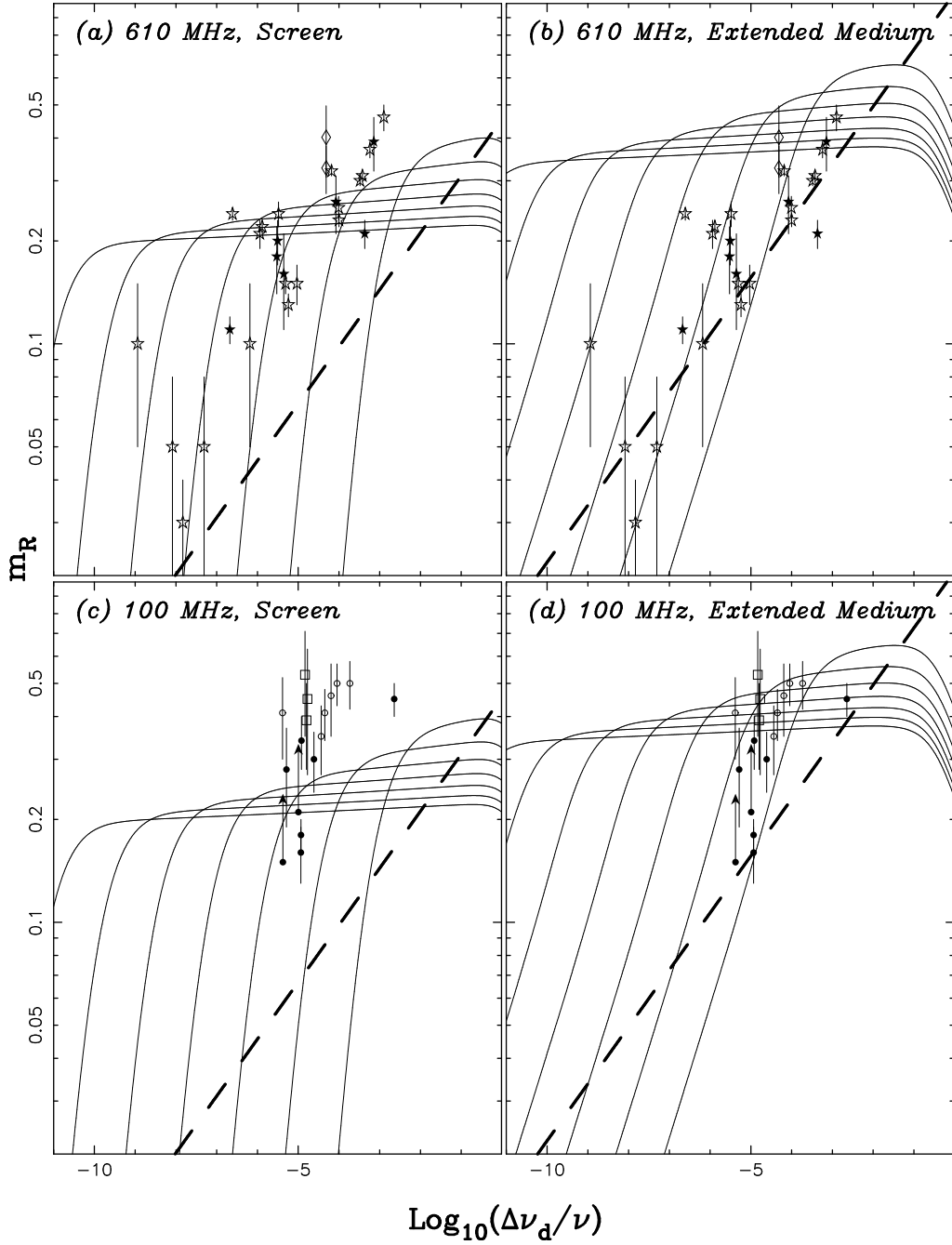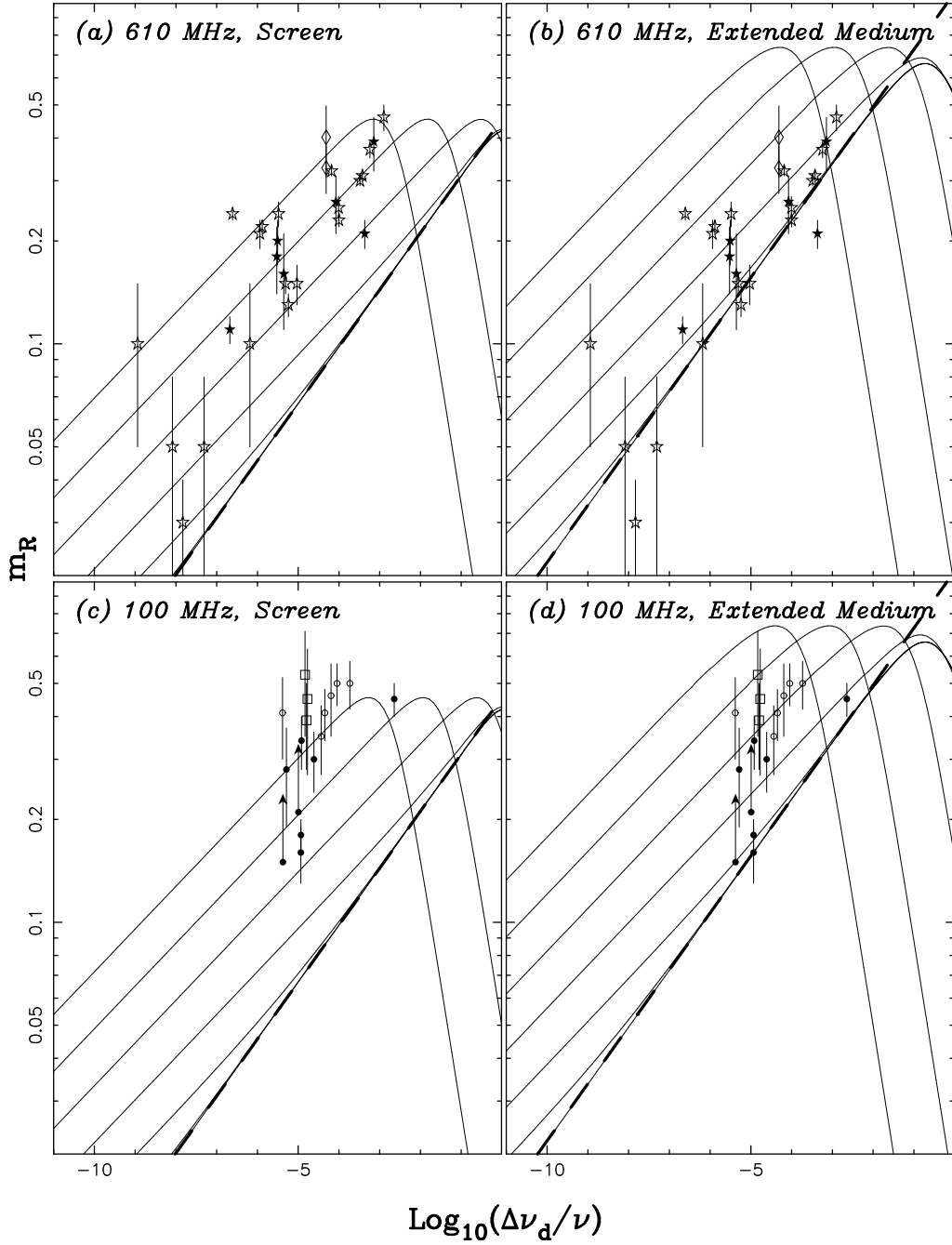
Fig. 6.— Theoretical and measured refractive scintillation indices, m_R, versus the normalized diffractive decorrelation bandwidth, $\Delta\nu_d/\nu$. (a) and (b) show measurements at 610 MHz; (c) and (d) correspond to measurements near 100 MHz. The solid curves give the theoretical results for the inner-scale model with a range of inner scales from 0 (corresponding to the simple Kolmogorov model) to The dashed line corresponds to the simple Kolmogorov model in the strong scattering limit. Panels (a) and (c)—screen geometry; panels (b) and (d)—uniform scattering medium.

15

requiring inner scale values (10^7m to 10^8m). The 610 MHz data in our analysis come from RISS observations of 21 pulsars made by Stinebring and are described in more detail by Smirnova et al. (1998), who also compare the results with various models for the spectrum and spatial distribution of the electron density. They note that 4 pulsars which are seen through known HII regions or supernovae remnants show relatively elevated values for m_R, and find 3 other pulsars with similar behavior. These are the points which lie above the Kolmogorov line in Figure 6b. Their interpretation is that for these objects the scattering is concentrated into regions either near the pulsar or near the Earth, and that these regions are characterized by an inner scale near 3×10^8m. Their spectrum model is very similar to our inner-scale model, except that the cut-off is characterized by a steep power-law rather than by an exponential function. We find a somewhat larger numerical value for the inner scale required to match those objects. We also note that the theoretical m_R values are consistently higher for an extended medium, and so require a more modest inner scale.

However, an important result of our analysis is an alternative explanation for the relatively high m_R values seen for some pulsars. We suggest that pulsar lines of sight can pass through discrete clouds with increased plasma density on large scales, that steepen the low-wavenumber spectrum as opposed to cutting off the high-wavenumbers. A discontinuity spectrum ($\beta = 4$) is one way that the spectrum can be steepened, but smoother structures on scales larger than 10^{11}m (~ 1 AU) would also boost the low-wavenumbers and could cause similar enhancements of refractive compared to diffractive scintillations. Such enhancements are likely to be associated with HII regions or supernova remnants. A similar idea was also discussed by Lestrade, Rickett, & Cognard (1998) in the context of extreme scattering events in pulsar timing measurements. To take this idea further, a composite between the Kolmogorov and the $\beta = 4$ or steeper spectra should be investigated, particularly one in which the line of sight is not uniformly weighted. Smirnova et al. (1998) also note that the strength of scattering increases very much faster with distance and dispersion measure than if the medium were statistically uniform. The distant pulsars in their sample are mostly observed at low galactic latitudes and so are subject to the enhanced density and turbulence described by the Tay-

lor & Cordes (1993) model. It appears that most distant pulsars follow the uniform extended Kolmogorov model with inner scale smaller than 10^6m. Thus although these lines of sight are subject to enhanced scattering in the inner galactic plane, the spectrum effectively follows the Kolmogorov law and the plasma is dispersed enough to approximate a uniform scattering medium. There are presumably discrete refracting structures present along these lines of sight, but their contribution to the density spectrum is masked by the higher densities of the inner Galaxy, which still follow an apparently turbulent spectral form.

6. SUMMARY AND CONCLUSION

In this paper, the theory of the $\beta = 4$ model for the electron density spectrum was derived for discontinuous density structures and compared with pulsar observations. A new feature of our analysis is the inclusion of an "outer scale" needed in any realistic model. The model is characterized by an effective exponent $\alpha(s)$ of the structure function, which remains between 1.95 and 1.6 over a very wide range of L_o values (cf. Figure 1). This at first seems a promising explanation for the spread in the estimates of α derived from VLBI observations of the angular broadening profile, as observed on heavily scattered lines of sight.

As discussed in section 4, from Figures 2 and 3, we find that the $\beta = 4$ model provides a somewhat better agreement with the measurements of the diffractive decorrelation bandwidth versus frequency for pulsar PSR B0833−45 (Vela) than does the simple Kolmogorov model. This might arise from refractive scattering effects caused in the supernova remnant associated with the Vela pulsar. Four other pulsars with decorrelation bandwidths measured against frequency show an appreciably stronger frequency dependence than the predictions of both the simple Kolmogorov and $\beta = 4$ models. However, there are substantial inconsistencies among the measurements and better observations are clearly needed, especially in view of the variability in $\Delta\nu_d$ documented by Bhat at al. (1999c).

The predictions of the $\beta = 4$ model for the variation of the refractive scintillation index with the diffractive decorrelation bandwidth are in partial agreement with the observations. As discussed in section 5, the values of m_R measured near 100 MHz are above the prediction of the simple Kolmogorov model and had previously been explained as the effect of an inner

TABLE 1

REFRACTIVE MODULATION INDEX DATA AT 610 MHz FROM THE LITERATURE.

Reference	Pulsar	Distance kpc	ν MHz	$\Delta\nu$ MHz	m_r	δm_r
Rickett & Lyne (1990)	B0531+21	2.0	610.0	2.96×10^{-2}	0.327	0.052
	B0531+21	2.0	610.0	2.96×10^{-2}	0.402	0.095
Kaspi & Stinebring (1992)	B0329+54	1.4	610.0	0.44	0.39	0.07
	B0833−45	0.55	610.0	1.29×10^{-4}	0.11	0.01
	B1749−28	1.2	610.0	5.13×10^{-2}	0.26	0.05
	B1911−04	2.29	610.0	1.91×10^{-3}	0.20	0.03
	B1933+16	7.8	610.0	1.82×10^{-3}	0.18	0.04
	B2111+46	5.22	610.0	2.69×10^{-3}	0.16	0.05
	B2217+47	2.31	610.0	0.26	0.21	0.02
Stinebring et al. (1999)	B0136+57	2.9	610.0	5.7×10^{-3}	0.15	0.02
	B0329+54	1.4	610.0	0.350	0.37	0.02
	B0525+21	2.3	610.0	0.30	0.31	0.01
	B0531+21	2.0	610.0	4.0×10^{-2}	0.32	0.01
	B0736−40	2.1	610.0	9.0×10^{-6}	0.03	0.01
	B0740−28	1.9	610.0	3.5×10^{-3}	0.13	0.01
	B0818−13	2.5	610.0	0.061	0.23	0.01
	B0833−45	0.5	610.0	1.50×10^{-4}	0.24	0.01
	B0835−41	4.2	610.0	7.0×10^{-4}	0.21	0.02
	B1641−45	4.6	610.0	7.0×10^{-7}	~0.1	0.05
	B1642−03	0.5	610.0	0.770	0.46	0.04
	B1749−28	1.5	610.0	6.0×10^{-2}	0.25	0.02
	B1818−04	1.6	610.0	4.0×10^{-4}	~0.1	0.05
	B1859−03	8.1	610.0	5.0×10^{-6}	~0.05	0.03
	B1911−04	3.2	610.0	8.0×10^{-4}	0.22	0.01
	B1933+16	3.5	610.0	2.0×10^{-3}	0.24	0.02
	B1946+35	7.9	610.0	3.0×10^{-5}	~0.05	0.03
	B2111+46	5.0	610.0	3.0×10^{-3}	0.15	0.01
	B2217+47	2.5	610.0	0.20	0.30	0.01

TABLE 2

REFRACTIVE MODULATION INDEX DATA AT 100 MHz FROM THE LITERATURE.

Reference	Pulsar	Distance kpc	ν MHz	$\Delta\nu$ MHz	m_r	δm_r
Cole et al. (1970)	B0809+74	0.31	81.5	1.38×10^{-3}	0.45	0.18
	B0834+06	0.72	81.5	1.3×10^{-3}	0.39	0.11
	B1919+21	0.66	81.5	1.2×10^{-3}	0.53	0.18
Helfand et al. (1977)	B0329+54	1.4	156.0	5.7×10^{-3}	0.35	0.08
	B0823+26	0.38	156.0	1.0×10^{-2}	0.46	0.11
	B1133+16	0.27	156.0	2.9×10^{-2}	0.50	0.08
	B1508+55	1.93	156.0	7.0×10^{-3}	0.41	0.07
	B1919+21	0.66	156.0	1.4×10^{-2}	0.50	0.07
	B2217+47	2.31	156.0	6.45×10^{-4}	0.41	0.11
Gupta et al. (1993)	B0329+54	1.4	73.8	3.1×10^{-4}	>0.15	$\cdots$
	B0809+74	0.31	73.8	8.90×10^{-4}	0.34	0.06
	B0834+06	0.72	73.8	8.6×10^{-4}	0.16	0.03
	B0950+08	0.12	73.8	0.17	0.45	0.05
	B1133+16	0.27	73.8	1.6×10^{-3}	0.18	0.02
	B1237+25	0.56	73.8	1.8×10^{-3}	0.30	0.06
	B1508+55	1.93	73.8	3.8×10^{-4}	0.28	0.09
	B1919+21	0.66	73.8	7.5×10^{-4}	>0.21	$\cdots$

scale, substantially larger than the values invoked by Spangler & Gwinn 1990. However, the measurements are also consistent with the $\beta = 4$ model with suitable choices of the outer scale. For the 610 MHz data, most of the measured m_R values are in good agreement with the prediction of the simple Kolmogorov model for the extended medium, and they lie below the curves of the $\beta = 4$ model. However, there are a significant number of good-quality observations, which lie somewhat above the Kolmogorov line. We suggest an alternative to a large inner scale on those lines of sight, that they pass through regions of enhanced density, which cause enhanced refractive scattering; these regions must have less small-scale substructure than in a turbulent medium and could include discontinuities.

Based on the above considerations, we reject the $\beta = 4$ model as a universal spectral model for the interstellar electron density fluctuations. The corollary is to strengthen the evidence for the Kolmogorov density spectrum, which in turn suggests a turbulent process in the interstellar plasma. However, the simple Kolmogorov spectrum is not a universal model either, since it disagrees with several of the m_R observations. Since the $\beta = 4$ model provides reasonable agreement for many of these discrepant observations, we propose that enhancements in the large scale part of the spectrum (which need not be described by discontinuities in density) occur on these lines of sight. With such enhancements causing the increase in refractive scintillation, there is no need to invoke the relatively large inner scales proposed by Coles et al. (1987). As proposed by Spangler & Gwinn (1990), a relatively small inner scale is then likely, controlled by the ion inertial length or Larmor radius.

It appears that different spectral models need to be considered for different lines of sight. A widely distributed turbulent plasma with occasional large ionized structures that increase the effective average power density, P_{N_e}, at low wavenumbers (large scales: 10^{11} m to 10^{14} m) is thus a model that needs further formal investigation. Very similar conclusions have been reached by Lestrade et al. (1998) and by Bhat et al. (1999b,c). This model could also explain the occasional "extreme scattering events" and episodes of fringes in dynamic spectra when a line of sight passes through a particular discrete density enhancement. New theoretical work is needed to quantify the expected statistics of these propagation events. It is likely that numerical modeling will be necessary to model non-stationary scattering media.

A. THEORY FOR REFRACTIVE SCINTILLATION INDEX

Screen Geometry

Here we derive expressions for the refractive modulation index, m_R, as a function of the normalized diffractive decorrelation bandwidth, $\Delta\nu_d/\nu$, for the inner-scale and $\beta = 4$ models. The simple Kolmogorov model is included as a special case where the inner scale goes to zero. A general integral expression for the refractive scintillation index is given by equation (10). With the medium concentrated into a thin layer (thickness Δz at z_p from the source) and an assumption of isotropy in the density spectrum, the equation becomes:

$$
\begin{aligned}
m_R^2 &= \frac{16\pi^2 r_e^2 c^2 \Delta z}{\nu^2} \int_0^\infty P_{N_e}(\kappa) \exp\left[-D_\phi(r_{\mathrm{F,scr}}^2 \kappa)\right] \\
&\times \sin^2\left(\frac{r_{\mathrm{F,scr}}^2 \kappa^2}{2}\right) \kappa \, d\kappa .
\end{aligned} \tag{A1}
$$

For both the inner-scale and $\beta = 4$ models, the exponential function in equation (A1) may be approximated by the Gaussian (Coles et al. 1987):

$$
\exp\left[-D_\phi(r_{\mathrm{F,scr}}^2 \kappa)\right] \simeq \exp\left[-(r_{\mathrm{F,scr}} u_{\mathrm{scr}})^2 \kappa^2\right] , \tag{A2}
$$

where $r_{\mathrm{F,scr}}$ is the Fresnel scale and u_{scr} is the strength of scattering, as defined in section 5. We now substitute models for the density spectrum $P_{N_e}(\kappa)$, given by equations (1) (with $\kappa_o = 0$) and (2) and obtain relations between m_R and the scattering measure $SM = C_{N_e}^2 \Delta z$. To these we add the connections between SM and $s_{0,\mathrm{scr}}$, for each spectral model, from the equations for the phase structure functions (17), (11), and (21) of LR99.

For the inner-scale model, we obtain:

$$
\begin{aligned}
\frac{8\pi^2 r_e^2 c^2 SM}{\nu^2} &= \frac{\alpha 2^\alpha}{s_{0,\mathrm{scr}}^\alpha} \frac{\Gamma(1+\alpha/2)}{\Gamma(1-\alpha/2)} \times \\
&\left[1 + \left(\frac{L_i}{s_{0,\mathrm{scr}}}\right)^\alpha \mu_\alpha\right]^{(2-\alpha)/\alpha} \tag{A3}
\end{aligned}
$$

where

$$
\mu_\alpha = \left[\frac{\alpha}{2}\Gamma\left(1+\frac{\alpha}{2}\right)\right]^{\alpha/(\alpha-2)} . \tag{A4}
$$

18

Table 3: Symbols Used

Symbols	Definition
$\alpha, \alpha(s)$	Exponent of separation s in structure function
β	Exponent of wavenumber in density power spectrum
$\boldsymbol{\beta}, \boldsymbol{\beta}'$	Vector spatial offsets in Appendix B
c	speed of light
C_1	Constant in uncertainty relation, $2\pi\Delta\nu_d\tau_d = C_1$
$C_{N_e}^2$	Coefficient in electron-density wavenumber spectrum $(\mathrm{m}^{-20/3})$
D_ϕ, D'_ϕ	Wave/phase structure function and its longitudinal gradient Equation (6)
D_S	Wave/phase structure function for a point (spherical wave) source
Δz	Screen or layer thickness
$\Delta\nu_d$	Diffractive Decorrelation Bandwidth
ϵ	Fractional frequency difference $|k_1 - k_2|/(k_1 + k_2)$
$f(r), f_0$	Radial profile function for electron density, interior density
$F(q)$	Three-dimesnsional Fourier Transform of $f(r)$ Equation (3)
$g(\eta), g_1(\eta)$	Intermediate functions of $\eta = \kappa^2$
J_0	Zero-order Bessel function of the first kind
κ	Transverse (2-dimensional) wavenumber
κ_i, κ_o	High and low wavenumber cutoffs Equation (1)
$k = 2\pi/\lambda, k_1, k_2$	Radio wavenumbers
k_m	Geometric mean of k_1, k_2
L	Pulsar distance
L_i, L_o	Inner and Outer scales
λ	Radio wavelength
m_R	Scintillation index (rms/mean) for refractive scintillation Equation (10)
m_{int}	Scintillation index due to scales intermediate between diffractive and refractive
n_0	Spatial number density of discontinuous objects
ν	Radio frequency
$P_{N_e}(q)$	Wavenumber spectrum for the electron density Equation (1)
q	Three-dimensional wavenumber
r_e	Classical electron radius
$r_{\mathrm{F},L}$	Fresnel scale $(\sqrt{L/k})$ Equation (11)
$r_{\mathrm{F,scr}}$	Fresnel scale for a screen $(\sqrt{z_e/k})$ Equation (12)
s	Transverse separation
SM	Scattering measure = Line of sight integral of $C_{N_e}^2$
s_0	Field coherence scale
s_R	Refractive scintillation scale
τ_d	Pulse decay time to 1/e
u	Strength of scattering parameter $(= r_{\mathrm{F},L}/s_0)$ Equation (9)
v_d	Normalized decorrelation bandwidth Equation (9)
V_4	Sum of wave structure functions Equation (B1)
x, y	Normalized distances
z, z_p	Distance from pulsar along line of sight toward observer
z_o	Observer-screen distance
z_e	Effective screen observer-distance $= z_o z_p/L$
ζ	$(s_R\kappa_o)^2$

Then substituting for SM we obtain an integral for m_R^2, which can be solved analytically using standard techniques (see e.g. Appendix 2 of Rickett 1973):

$$m_R^2 = 2^\alpha\Gamma\left(1 + \frac{\alpha}{2}\right)\left[1 + \left(\frac{L_i}{s_{0,\mathrm{scr}}}\right)^\alpha \mu_\alpha\right]^{(2-\alpha)/\alpha} \times$$

$$\left[(\cos\psi)^{-\alpha/2}\cos(\psi\alpha/2) - 1\right] \times$$

$$\left[(L_i/2s_{0,\mathrm{scr}})^2 + u_{\mathrm{scr}}^4\right]^{\alpha/2}, \tag{A5}$$

where $u_{\rm scr} = r_{\rm F,scr}/s_{0,\rm scr}$, and ψ is given by:

$$\psi = \cot^{-1}\left[\left(\frac{L_i}{2s_{0,\rm scr}u_{\rm scr}}\right)^2 + u_{\rm scr}^2\right]. \qquad (A6)$$

We see that m_R depends on $u_{\rm scr}$ with $L_i/s_{0,\rm scr}$ as a parameter. Similarly the diffractive decorrelation bandwidth, $\Delta\nu_d/\nu$, depends on $u_{\rm scr}$ through equation (9) with v_d as a parameter, which is a very slow function of $L_i/s_{0,\rm scr}$ as discussed in section 4.

For the simple power-law model we set $L_i = 0$, and in the strong scattering limit ($u_{\rm scr} >> 1$), equation (A6) gives $\psi \approx u_{\rm scr}^{-2}$, and we obtain the asymptotic expression:

$$m_R^2 = \frac{\alpha 2^\alpha}{4}\left(1 - \frac{\alpha}{2}\right)\Gamma\left(1 + \frac{\alpha}{2}\right)\left(\frac{1}{u_{\rm scr}^2}\right)^{2-\alpha}. \quad (A7)$$

Putting this together for the simple Kolmogorov model with $\alpha = 5/3$, we have the simple relation: $m_R = 0.459(\Delta\nu_d/\nu)^{0.167}$, plotted as the thick dashed lines in the screen plots in Figures 5 and 6.

For the general inner-scale model, with L_i nonzero, we show computed curves in Figure 6. We can recognize two regimes. Consider first the case of small L_i. With sufficiently strong scattering, $s_{0,\rm scr} < L_i < r_{\rm F,scr}$, $m_R^2 \propto (L_i/u_{\rm scr}r_{\rm F,scr})^{2-\alpha}$. However, there is a complication in portraying this behavior in a plot versus $\Delta\nu_d/\nu$ for fixed inner scale, because of the variation of $r_{\rm F,scr}$ with distance, which is not specified by the horizontal variable $\Delta\nu_d/\nu$. We deal with this by obtaining an approximate scaling of $r_{\rm F,scr}$ with $\Delta\nu_d/\nu$. When $s_{0,\rm scr} < L_i$, equation (A3) relates $SM \propto s_{0,\rm scr}^{-2}$, or $SMr_{\rm F,scr}^2 \propto u_{\rm scr}^2$. We now argue that on average $SM \propto$ pulsar distance $\propto r_{\rm F,scr}^2$, and eliminating SM, we see that, $r_{\rm F,scr} \propto u_{\rm scr}^{0.5}$. With these scalings and $s_{0,\rm scr} < L_i < r_{\rm F,scr}$, we see:

$$\begin{aligned}
m_R^2 &\propto (L_i/u_{\rm scr}r_{\rm F,scr})^{2-\alpha} \propto (L_i/r_{\rm F,ref}u_{\rm scr}^{1.5})^{2-\alpha} \\
&\propto u_{\rm scr}^{-0.5} \propto (\Delta\nu_d/\nu)^{0.25}. \qquad (A8)
\end{aligned}$$

Here $r_{\rm F,ref}$ is the Fresnel scale for a "reference" pulsar, and the last version in equation (A8) comes from using the Kolmogorov exponent $\alpha = 5/3$, which gives the asymptotic slope of $1/8$ for curves at the lower left of Figure 6. Now with L_i and $r_{\rm F,scr}$ fixed, let $s_{0,\rm scr}$ increase (i.e. less scattering) until $L_i < s_{0,\rm scr} < r_{\rm F,scr}$. The inner scale is no longer important, and we get the same relation as for the simple Kolmogorov spectrum: $m_R^2 \propto u_{\rm scr}^{-2(2-\alpha)} \propto (\Delta\nu_d/\nu)^{1/3}$; visible where the curves steepen with increasing $\Delta\nu_d/\nu$.

For larger inner scales, the curves in Figure 6 show a pronounced peak. These occur for inner scales greater than the Fresnel scale and will be associated with focusing and caustics. Since our treatment only includes the first order term in the low wavenumber expansion, it is not reliable in the region of the peak. Goodman et al. (1987) have discussed caustics at length for the same inner-scale spectrum. They note that when $s_{0,\rm scr} < r_{\rm F,scr} < L_i < s_R$, the scintillation power spectrum starts to fill in at scales intermediate between the diffractive and refractive wavenumbers. Their equation (2.5.7) gives an estimate of the variance in this extra term as:

$$\begin{aligned}
m_{\rm int}^2 &\sim 2(L_i/s_R)^2\ln(L_i/s_{0,\rm scr}) \\
&\sim 2(L_i/u_{\rm scr}r_{\rm F,scr})^2\ln(L_iu_{\rm scr}/r_{\rm F,scr}).(A9)
\end{aligned}$$

With fixed L_i, $m_{\rm int}^2$ increases much more steeply with decreasing $u_{\rm scr}$ than does m_R^2. Thus as $u_{\rm scr}r_{\rm F,scr}$ decreases, there are fewer and fewer independent phase perturbations across the scattering disc. When $u_{\rm scr}r_{\rm F,scr} \sim L_i$, focusing represented by $m_{\rm int}^2 \sim 4\ln(L_i/r_{\rm F,scr}) > 1$ occurs. We note that the theoretical m_R versus ν_d/ν plots in Gupta et al. (1993) omit the focusing condition and are wrong for inner scales greater than the Fresnel scale. The effect of higher order terms in the low-wavenumber expansion has been studied by Dashen & Wang (1993). They obtain a more efficient expansion scheme that gives improved accuracy near the peak in scintillation index. Nevertheless, it seems that a reliable prediction for the behavior near the peak in scintillations requires numerical evaluation. This becomes even more necessary in treating an extended scattering medium.

We also note that the drop in m_R as scattering gets weaker past the peak in Figure 6 is real. It represents the fact that when a square-law structure function applies for scales from $s_{0,\rm scr}$ up to the scattering disc size, there is insufficient phase curvature and the scintillations remain weak even though $u_{\rm scr} > 1$. In such circumstances the "scattering disc" is a misnomer, since an observer would see only a single angle of arrival, that could wander over a region of scale $u_{\rm scr}r_{\rm F,scr}$.

Turning to the screen analysis of the $\beta = 4$ model, we relate $s_{0,\rm scr}$ to SM using equation (21) from LR99, where the phase structure function equals one. This gives the following analog of equation (A3) for the

inner-scale model:

$$\frac{\pi^2 r_{\mathrm{e}}^2 c^2 SM}{\nu^2} = \left\{ s_{0,\mathrm{scr}}^2 \ln \left[1 + 4 \left(\frac{L_o}{s_{0,\mathrm{scr}}} \right)^2 \right] \right\}^{-1} .$$
(A10)

Substituting the $\beta = 4$ model for the density spectrum in equation (A1) and letting $\eta = \kappa^2$, we obtain:

$$m_R^2 = \frac{8\pi^2 r_{\mathrm{e}}^2 c^2 SM}{\nu^2} \int_0^\infty \frac{1}{(\eta + \kappa_o^2)^2} \times$$
$$\exp[-(r_{\mathrm{F,scr}} u_{\mathrm{scr}})^2 \eta] \, \sin^2(r_{\mathrm{F,scr}}^2 \eta / 2) \, d\eta \quad \text{(A11)}$$

In order to evaluate this integral, we let $g(\eta)$ represent the integrand, and we let $g_1(\eta)$ be the same as $g(\eta)$ but with κ_o set equal to zero. We can then rewrite the integral in equation (A11) as:

$$m_R^2 = 8 \left\{ s_{0,\mathrm{scr}}^2 \ln \left[1 + (2L_o / s_{0,\mathrm{scr}})^2 \right] \right\}^{-1} \times$$
$$\left\{ \int_0^\infty g_1(\eta) d\eta - \int_0^\infty [g_1(\eta) - g(\eta)] d\eta \right\} \quad \text{(A12)}$$

The first integral can be evaluated analytically (see e.g. Gradshteyn & Ryznhik 1965). In strong scattering, the exponential term cuts off the oscillations of the sine term, which can be approximated by its argument, and the $g_1(\eta) - g(\eta)$ becomes negligible for values of η larger than κ_o^2. With these approximations we can also do the second integral. Putting these together, we obtain:

$$m_R^2 = \left\{ \ln[1 + (2L_o / s_{0,\mathrm{scr}})^2] \right\}^{-1} \times$$
$$\left\{ 4 u_{\mathrm{scr}}^2 \tan^{-1}(u_{\mathrm{scr}}^{-2}) - 2 u_{\mathrm{scr}}^4 \ln(1 + u_{\mathrm{scr}}^{-4}) - \right.$$
$$\left. 2\zeta \left[(2 + \zeta) \, e^\zeta \, \mathrm{E}_1(\zeta) - 1 \right] \right\} , \quad \text{(A13)}$$

where E_1 is the exponential integral, $\zeta = (s_0 \kappa_o)^2 u_{\mathrm{scr}}^4 = (s_R \kappa_o)^2$. In the latter form $s_R = r_{\mathrm{F,scr}} u_{\mathrm{scr}}$ is the refractive scale (equal to scattering disk radius). Again, m_R is related to $\Delta\nu_d/\nu$ through: $\Delta\nu_d/\nu = v_d/u_{\mathrm{scr}}^2$. The resulting curves are shown in the screen panels of Figure 5. Consider the asymptotic behavior for m_R^2 in equation (A13) as a function of u_{scr}. As the strength of scattering u_{scr} increases, $\Delta\nu_d/\nu$ decreases ($\propto u_{\mathrm{scr}}^{-2}$). In equation (A11), the exponential term cuts off the integral (at $1/s_R^2$) before the oscillations of the $\sin^2$ Fresnel filter, which then approximates $\eta^2 r_{\mathrm{F,scr}}^4 / 4$. If also $\zeta = (s_R \kappa_o)^2 \ll 1$, we can ignore κ_o^2 in the denominator and the remaining η^{-2} cancels the η^2 from the Fresnel filter, and the integral depends only on $1/s_R$. In this approximation, m_R^2 is then simply proportional to the slowly varying logarithmic term, which

explains the relatively flat part of the curves in Figure 5; under these conditions, in equation (A13) the first two terms in the curly brackets sum to 2 and the last term is negligible. With L_o fixed, now let u_{scr} increase, making s_R increase. Eventually ζ becomes greater than one when the scattering disk becomes greater than the outer scale. At this point the exponential term cuts off the integral below κ_o^2, where the spectrum flattens. As u_{scr} increases even further, the integral decreases steeply, causing the down-turn at very small $\Delta\nu_d/\nu$. We again note that our expressions rely on the first order of an expansion and will not be reliable near the peak in the scintillation index. However, there is not the same focusing condition that applied for very large inner scales.

Extended Scattering Medium

In order to obtain expressions for m_R for the two spectrum models in the *uniform* extended medium geometry, we must complete the line-of-sight integrals in equation (10) in addition to following the steps used in the screen geometry. For each distance $x = z/L$ in the line of sight, there is also an integration over variable y in the exponential cut-off. If $D'(s) \propto s^\alpha$, this y-integration yields $LD'(\kappa r_{F,L}^2 x(1-x))/(\alpha+1)$, where $r_{\mathrm{F},L} = \sqrt{Lc/(2\pi\nu)}$. This again provides a low-pass cut-off at the reciprocal of the radius of the effective scattering disk, where $\kappa \sim (u_S r_{\mathrm{F},L})^{-1}$. We define the scattering strength by $u_S = r_{\mathrm{F},L}/s_{0_S}$, with the field coherence scale s_{0_S}, as in LR99, defined where the spherical wave structure function equals unity, measured in the observing plane. For the other spectrum models there is not such a simple relation for the y-integration, but there is still an effective cutoff given by a similar equation. When the x-integration is completed, the effective Fresnel scale is actually smaller than $r_{\mathrm{F},L}$ due to averaging over the $\sqrt{x(1-x)}$.

In analogy with the screen geometry, we make use of identities similar to those given by equations (A3) and (A10). For the extended medium, these identities are in turn derived from the *wave* structure functions for the inner-scale and $\beta = 4$ models (cf. LR99). The identities obtained thus will be similar to those for the screen geometry, except that for the inner-scale model, (1) there will be a factor of 3 on the right side of equation (A3), and (2) the 1 in square brackets is replaced by $[3/(1 + \alpha)]^{\alpha/(\alpha-2)} \approx 1.8$ for the Kolmogorov exponent. For the $\beta = 4$ model, the only change will be a factor of 3 on the right side of equation (A10). We use all of the aforementioned identi-

ties for the inner-scale and $\beta = 4$ models and compute the x integral numerically, since it cannot be carried out analytically.

The shapes of the curves bear a close relationship to the screen results, though the extended medium values generally lie above the associated screen values at the same $\Delta\nu_d/\nu$.

B. Diffractive Intensity Correlation Function

The second moment of intensity is needed to describe the fluctuations of intensity. Under strong scintillation conditions, separate forms can be used for refractive and diffractive fluctuations, since their spatial scales differ by several orders of magnitude. In LR99, as elsewhere in the ISS literature, the correlation of diffractive scintillations is approximated by the squared magnitude of the second moment of the field, leading to the simple result that the spatial scale of the diffractive scintillations is equal to the scale where the phase structure function equals unity (s_0). However, Goodman and Narayan (1985) showed that for steep spectra ($\beta > 4$) this is no longer the case and the diffractive scale can be larger than s_0. Here we examine this question for the $\beta = 4$ spectrum. We give the details for a phase screen with plane wave source, which are readily generalized to a spherical wave source.

The two-frequency intensity cross-spectrum at wavenumber $\boldsymbol{\kappa}$ for a screen at distance L is given by the Fourier-like integral equation (17) of CCFFH. This depends on the combination of structure functions V_4, which for a plasma screen can be written as:

$$V_4 = \frac{k_m^2}{k_1^2} D_\phi(\boldsymbol{\kappa}\frac{L}{k_1}) + \frac{k_m^2}{k_2^2} D_\phi(\boldsymbol{\kappa}\frac{L}{k_2}) - D_\phi(\frac{\boldsymbol{\kappa}L}{k_o} + \boldsymbol{\beta}')$$
$$-D_\phi(\frac{\boldsymbol{\kappa}L}{k_o} - \boldsymbol{\beta}') + D_\phi(\boldsymbol{\beta}' + \frac{\boldsymbol{\kappa}\epsilon L}{k_o}) + D_\phi(\boldsymbol{\beta}' - \frac{\boldsymbol{\kappa}\epsilon L}{k_o}) , \text{(B1)}$$

where k_1 and k_2 are the two radio wavenumbers, k_m is their geometric mean, $\bar{k}$ is their arithmetic mean, $k_o = k_m^2/\bar{k}$, $\epsilon = |k_1 - k_2|/2\bar{k}$, and D_ϕ is evaluated at k_m; $\boldsymbol{\beta}'$ is a spatial offset which is the variable of integration.

Consider first the single frequency case $k_1 = k_2(\epsilon = 0)$. In the limit of very large κ, the first four structure functions saturate and sum to zero. The last two are equal and $V_4 \approx 2D_\phi(\beta')$, which gives the simple diffractive limit mentioned above. This is the zero-order term of an expansion, which is obtained in terms

of the sum of the first four terms as a small quantity. The zero order result requires full saturation, which requires $\kappa L/k_m \gtrsim L_o$. In diffractive scintillation $\kappa \sim 1/s_0$; hence, the condition becomes that the refractive scale $s_R = L/(k_m s_0) \gtrsim L_o$. Our concern here is to consider what happens when the diffractive κ is not large enough for saturation of D_ϕ. For shallow density spectra ($\beta < 4$), small argument approximations to the structure function follow an exponent $\beta - 2 < 2$, and the zero-order term gives a good approximation even when $s_R < L_o$. However, for steep spectra Goodman and Narayan (1985) showed that the leading term in the structure function follows a square law, which exactly cancels in V_4; the result is that the high wavenumber limit depends on the next term in the structure function expansion, which yields a diffractive scale that is greater than the scale s_0 (defined by the square law term).

Now we consider the case for $\beta = 4$ model, when the scattering disc s_R is smaller than the outer scale L_o. Here we can approximate equation (8) by:

$$D_\phi(s) = \frac{s^2}{s_0^2} - \frac{s^2 \ln(s^2/s_0^2)}{s_0^2 \ln(4/s_0^2 \kappa_o^2)} . \quad \text{(B2)}$$

As for the steep spectra, the leading term in the structure function follows a square law, which cancels when substituted into equation (B1). V_4 can then be approximated for large κ by expanding in $\beta' k_m/(\kappa L)$. The result is:

$$V_4 \sim \frac{2\beta'^2 [\ln(u^4) + 1 + 2\cos^2\theta - \ln(\beta'^2/s_0^2)]}{s_0^2 \ln(4/s_0^2 \kappa_o^2)} . \quad \text{(B3)}$$

Here u is the strength of scattering defined in equation (9); θ is the angle between vectors $\boldsymbol{\kappa}$ and $\boldsymbol{\beta}'$. We note that for a Kolmogorov spectrum in the high-wavenumber limit, V_4 also includes terms in $\cos^2\theta$, which would be accounted for in the higher order terms of the expansion. A result similar to equation (B3) is given by Dashen & Wang (1993), though for a 1-dimensional phase screen. In considering the spectrum of intensity fluctuations (eq. 17 of CCFFH), one can show that the dominant wavenumber is approximately $\kappa \sim \beta'^{-1}$ With these substitutions in V_4, which we then set $= 2$, we solve for β'; this gives an approximate equation for the diffractive spatial scale s_d:

$$s_d^2 \sim s_0^2 \frac{\ln(4/s_0^2 \kappa_o^2)}{\ln(u^4) + 2} . \quad \text{(B4)}$$

Under the condition assumed in this approximation, $s_R \ll L_o$, we find $s_d > s_0$. However, in practice the

ratio s_d/s_0 never becomes large. With a large outer scale, say $L_o = 3$ pc, and typical observing conditions $s_0 \sim 10^8$ m and $u \gtrsim 100$, we find $s_d \lesssim 1.7 s_0$. Thus the diffractive scale could be 70% greater than s_0 and would slowly approach s_0 for smaller outer scales.

Turning to the two-frequency intensity correlation ($0 < \epsilon \ll 1$) in the diffractive limit of large κ, the results of CCFFH still apply. Namely, that the last two terms of equation (B1) largely control the decorrelation versus frequency. They group the remaining terms into a filter that depends only on κ and a smaller term that becomes the basis of the expansion. The filter term was discussed by LR99 and shown to be important only as the strength of scattering decreases. It is the last two terms in V_4 that determine the zero-order result, so we looked at the effect of the higher order terms. The quantity that we are ultimately concerned with is the cross-correlation of intensity at offset frequencies at the same observing point. This comes from the integral of the cross-spectrum. Equations (31) through (34) of CCFFH give the zero and first order terms of the cross spectrum in terms of the spectrum of refractive index fluctuations in the layer. For the $\beta = 4$ spectrum we reduced these to a sum of confluent hypergeometric functions, which can be explicitly computed. For a sample observing condition we found that the higher order terms for the cross-spectrum itself were significant compared to the zero-order term; however when integrated to give intensity cross-correlation, they only had a minor effect on the decorrelation bandwidth itself ($\lesssim 5\%$ increase). The reason for this appears to be the dominant effect of the last two terms in the V_4 summation with unequal frequencies.

To summarize we find a modest (logarithmic) increase in the diffractive scale relative to the field coherence scale s_0, but that this remains less than a factor of 1.7 for the likely ISS parameters. This is accompanied by a smaller increase in the decorrelation bandwidth relative to the calculations of LR99, which relied on the normal zero-order expansion at high wavenumbers. This small offset in the decorrelation bandwidth is negligible compared to the measurement errors for the observations under consideration. We assume that the conclusions reached here for a screen would also apply for an extended scattering medium.

REFERENCES

Armstrong, J. W., Rickett, B. J., & Spangler, S. R. 1995, ApJ, 443, 209

Bhat, N. D. R., Gupta, Y., & Rao, A. P. 1998, ApJ, 500, 262

Bhat, N. D. R., Rao, A. P., & Gupta, Y. 1999a, ApJS, 121, 483

Bhat, N. D. R., Rao, A. P., & Gupta, Y. 1999b, ApJ, 514, 249

Bhat, N. D. R., Gupta, Y., & Rao, A. P. 1999c, ApJ, 514, 272

Biskamp, D. 1993, *Nonlinear Magnetohydrodynamics*, Cambridge Univ. Press, Cambridge, UK

Blandford, R., & Narayan, R. 1985, MNRAS, 213, 591

Codona, J. L., Creamer, D. B., Flatté, S. M., Frehlich, R. G., & Henyey, F. S. 1986, Radio Science, 21, No. 5, 805 [CCFFH]

Cole, T. W., Hesse, H. K., & Page, C. G. 1970, Nature, 225, 712

Coles, W. A., Frehlich, R. G., Rickett, B. J., & Codona, J. L. 1987, ApJ, 315, 666

Cordes, J. M., Weisberg, J. M., & Boriakoff, V. 1985, ApJ, 288, 221 [CWB]

Cordes, J. M., Pidwerbetsky, A., & Lovelace, R. V. E. 1986, ApJ, 310, 737

Cordes, J. M., & Wolszczan, A. 1986, ApJ, 307, L27

Cordes, J. M., Weisberg, J. M., Frail, D. A., Spangler, S. R., & Ryan, M. 1985, ApJ, 288, 221

Dashen, R., & Wang, G. Y. 1993, J. Opt. Soc. Am. A, 10, 1219

Fiedler, R. L., Dennison, B., Johnston, K. J., & Hewish, A. 1987, Nature, 326, 675

Goldreich, P., & Sridhar, S. 1995, ApJ, 438, 763

Goldreich, P., & Sridhar, S. 1997, ApJ, 485, 680

Goodman, J., & Narayan, R. 1985, MNRAS, 214, 519

Goodman, J., Romani, R. W., Blandford, R. D., & Narayan, R. 1987, MNRAS, 229, 73

Gradshteyn, I. S., & Ryzhnik, I. M. 1965, Table of Integrals, Series, and Products (New York: Academic Press)

Gupta, Y., Rickett, B. J., & Coles, W. A. 1993, ApJ, 403, 183

Gupta, Y., Rickett, B. J., & Lyne, A. G. 1994, MNRAS, 269, 1035

Gupta, Y., Bhat, N. D. R., & Rao, A. P. 1999 ApJ, in press

Helfand, D. J., Fowler, L. A., & Kuhlman, J. V. 1977, AJ, 82, 701

Higdon, J. C. 1984, ApJ, 285, 109

Higdon, J. C. 1986, ApJ, 309, 342

Johnston, S., Nicastro, L., & Koribalski, B. 1998, MNRAS, 297, 108

Kaspi, V. M., & Stinebring, D. R. 1992, ApJ, 392, 530

Lambert, H. C. 1998, Interstellar Electron Density Spectra, PhD Thesis, University of California, San Diego

Lambert, H. C., & Rickett, B. J. 1999, submitted to ApJ[LR99]

Lestrade, J-F, Rickett, B. J., & Cognard, I. 1998, A&A, 334, 1068

Minter, A. H., & Spangler, S. R. 1997, ApJ, 485, 182

Narayan, R. 1992, Phil. Trans. R. Soc. London A, 341, 151

Papoulis, A. 1991, Probability, Random Variables, and Stochastic Processes, Third Edition (New York: McGraw-Hill Inc.)

Pouquet, A. 1978, J. Fluid Mech., 88, 1

Prokhorov, A. M., Bunkin, F. V., Gochelashvily, K. S., & Shishov, V. I. 1975, Proc. IEEE, 63, 790

Ratcliffe, J. A. 1956, Reports on Progress in Physics 19, 188

Rickett, B. J. 1973, J. Geophys. Res., 78, 1543

Rickett, B. J. 1977, ARA&A, 15, 479

Rickett, B. J., Coles, W.A., & Bourgois, G. 1984, A&A, 134, 390

Rickett, B. J., & Lyne, A. G. 1990, MNRAS, 244, 68

Rickett, B. J., Lyne, A. G., & Gupta, Y. 1997, MNRAS, 287, 739

Rickett, B. J., Coles, W. A., & Markkanen, J. 1999, submitted to ApJ

Roberts, J. A., & Ables, J. G. 1982, MNRAS, 201, 1119

Romani, R. W., Narayan, R., & Blandford, R. 1986, MNRAS, 220 19

Smirnova, T. V., Shishov, V. I., & Stinebring, D. R. 1998, Astronomical Reports, 42, 766

Spangler, S. R., & Gwinn, C. R. 1990, ApJ, 353, L29

Spangler, S. R. 1991, ApJ, 376, 540

Spangler, S. R. 1999, ApJ, 522, 879

Sridhar, S., & Goldreich, P. 1994, ApJ, 432, 612

Stinebring, D. R., Smirnova, T. V., Hovis, J., Kempner, J. C., Myers, E. B., Hankins, T. H., Kaspi, V. M., & Nice, D. J. 1996, in "Pulsars: Problems and Progress", Ed. Johnston, S., Walker, M. A., & Bailes, M., Proceedings of IAU Colloquium 160, ASP Conference Series, 105, 455

Tatarskii, V. I. 1961, Wave Propagation in a Turbulent Medium (New York: Dover Publications)

Taylor, J. H., & Cordes, J. M. 1993, ApJ, 411, 674

Taylor, J. H., Manchester, R. N., & Lyne, A. G. 1993, ApJS, 88, 529

Trotter, A. S., Moran, J. M., & Rodríguez, L. F. 1998, ApJ, 493, 666